TOWARDS UNDERSTANDING THE CATALYTIC BOND-BREAKING SEQUENCES OF POLYOL OXIDATION ON PD(111) SINGLE CRYSTAL MODEL CATALYSTS

A THESIS SUBMITTED TO THE GRADUATE SCHOOL OF ENGUNEERING AND SCIENCE OF BILKENT UNIVERSITY IN PARTIAL FULFILLMENT OF THE REQUIREMENTS FOR THE DEGREE OF MASTER OF SCIENCE IN CHEMISTRY

By

Ömer Faruk Sadak

September 2023

TOWARDS UNDERSTANDING THE CATALYTIC BOND-BREAKING SEQUENCES OF POLYOL OXIDATION ON PD(111) SINGLE CRYSTAL MODEL CATALYSTS

By Ömer Faruk Sadak

September 2023

We have certified that we have read this dissertation and that in our opinion it is fully adequate, in scope and quality, as a dissertation for the degree of Master of Science.

Emrah Özensoy (Advisor)

Şefik Süzer

Sarp Kaya

Approved for the Graduate School of Engineering and Science:

ABSTRACT

TOWARDS UNDERSTANDING THE CATALYTIC BOND-BREAKING SEQUENCES OF POLYOL OXIDATION ON PD(111) SINGLE CRYSTAL MODEL CATALYSTS

By Ömer Faruk Sadak

M.Sc. in Chemistry

Advisor: Emrah Özensoy

September 2023

Understanding the bond-breaking sequences of catalytic polyol oxidation on transition metal catalysts is critical for the chemical transformation of biomass derived chemical feedstock into value-added products which may also offer new alternatives to fossil fuel-based commodity chemicals. In the current work, oxidation of ethylene glycol on an atomically well-defined Pd(111) single crystal planar model catalysts was investigated via temperature programmed desorption (TPD) technique under ultra-high vacuum (UHV) conditions. Presence of surface oxygen atoms was found to promote the formation of formaldehyde (H_2CO) and carbon dioxide as the most prominent catalytic oxidation products. Enhancement in formaldehyde generation was observed upon increasing the ethylene glycol-to-oxygen ratio. Our results indicate that the activation of C-C bonds was primarily facilitated by atomic oxygen, preceding the complete dehydrogenation of the $C_2H_xO_z$ surface species. The formation of H_2CO was mainly attributed

to the most unstable surface species in terms of C-C bond scission, namely -OCH_2CO- and -OCH_2CHO-. Other surface species such as -OCHCHO- and -OCHCO- led to additional decomposition products such as CO rather than formaldehyde.

Keywords: Partial Oxidation, Ethylene Glycol, Formaldehyde, Selective Oxidation, Pd(111), Model Catalyst

ÖZET

PD(111) TEK KRİSTAL MODEL KATALİZÖRLER ÜZERİNDEKİ POLİOL OKSİDASYONLARININ KATALİTİK BAĞ KIRILMA DİZİLERİNİN İNCELENMESİ

Ömer Faruk Sadak

Kimya, Yüksek Lisans

Tez Danışmanı: Emrah Özensoy

Eylül 2023

Katalitik poliol oksidasyonunun, geçiş metal katalizörler üzerindeki bağ koparma dizilerini anlamak, biyokütle türevi kimyasal hammaddeyi değerli ürünlere dönüştürmede ve aynı zamanda fosil yakıt temelli yeni ticari kimyasalların geliştirilmesi için yeni alternatifler sunabilir. Bu çalışmada, etilen glikolün atomik düzeyde iyi tanımlanmış Pd(111) tek kristal düzlemsel model katalizör üzerinde sıcaklık programlı desorpsiyon (TPD) tekniği kullanılarak oksidasyonu, ultra yüksek vakum (UHV) koşullarında incelenmiştir. Yüzeydeki oksijen atomlarının, formaldehit (H_2CO) ve karbondioksit oluşumunu, en belirgin katalitik oksidasyon ürünleri olarak ortaya çıkardığı tespit edilmiştir. Formaldehit üretiminin, etilen glikol'ün oksijene oranının artırılmasıyla arttığı gözlemlenmiştir. Sonuçlarımız, C-C bağlarının aktivasyonunun, öncelikle atomik oksijen tarafından kolaylaştırıldığını ve $C_2H_xO_z$ yüzey türlerinin tam dehidrojenasyonundan önce gerçekleştiğini göstermektedir. H_2CO'nun oluşumu, C-C bağ kırılması açısından en kararsız yüzey türlerine, yani -OCH_2CO- ve -OCH_2CHO-

türlerine dayandırılmıştır. -OCHCHO- ve -OCHCO- gibi diğer yüzey türleri, formaldehit yerine CO gibi farklı başka ayrışma ürünlerine yol açmıştır.

Anahtar Sözcükler: Biyokütle Kullanımı, Etilen glikol, Formaldehit, Seçici oksidasyon, Pd(111), Model Katalizör

Acknowledgements

First and foremost, I would like to express my gratitude to Prof. Emrah Özensoy, who has provided both guidance and mentorship over the past 7 years. From my first year at university, he has exemplified the qualities of a true academic and ethical role model, teaching me through his actions what it means to be a scholar. I take pride in being his student, knowing that the lessons he imparted will accompany me throughout my life as a scientist.

I extend my thanks to my thesis committee members: Prof. Şefik Süzer, and Assoc. Prof. Sarp Kaya for their valuable insights and constructive criticism.

I would also like to acknowledge Dr. Igor Lyubinetsky, who, over the course of two years, taught me the intricacies of research methodology and experimental design, drawing from his extensive experiences. Additionally, I am grateful to Dr. Yusuf Koçak, who has consistently provided support and calmly helped me navigate challenges. I also offer my appreciation to Dr. Ahsan Jalal, who has been both a big brother and a post-doc colleague during his time here.

To Arca Anıl, my partner in the ups and downs of our graduate journey, I am profoundly grateful for the shared experiences and companionship. Thanks to Arca and Eylül Ergün, I have not only safeguarded my mental well-being but also learned to view the world through a more rational and diverse lenses. With the knowledge that our paths will cross again, I wish both Arca and Eylül a rewarding doctoral adventure.

To my fellow companions on this journey and to each member of the Özensoy laboratory, I extend my heartfelt thanks. Special appreciation goes to Berk Delibaş, who has been by my side since our undergraduate years and whom I will consider a brother for life; to Gözde Karaoğlu, with whom I have shared countless discussions about life in the lab over the past year; to Yağmur Altınkaynak, who has played an irreplaceable role in my academic

journey; to Beyza Erdivan, Ayşe Dilay Erdalı and Kaan Karaca who have helped alleviate our shared stresses.

Lastly, I am indebted to my parents, who have supported me in every way possible, guiding me to this point. The positive aspects of my profession and personality are a direct result of your efforts. I am committed to honoring you through meaningful accomplishments in the chapters of my life that lie ahead.

Table of Contents

List of Figures

Chapter 1

1 Introduction

1.1 Renewable Biomass: A Vital Pathway for Environmentally Friendly Chemical Production

The adoption of renewable resources is rapidly evolving into a necessity, surpassing a mere preference. This transformation is propelled by two fundamental factors: the finite nature of fossil fuel reserves and their detrimental ecological repercussions. Within this context, plant biomass emerges as a preeminent renewable feedstock, showcasing immense potential due to its capacity for efficient conversion into both fuels and chemicals within the realm of biorefineries.[1]–[3] Furthermore, an intriguing trend is observed in the price dynamics of corn-to-oil, exhibiting a consistent decline over the span of the last six decades. This reduction has been striking, transitioning from a ratio of 5 to a level below 1, as visually represented in Figure 1.1.[4] Such a profound shift amplifies the attractiveness of biomass utilization to unprecedented levels. Nonetheless, to position biomass conversion as a viable alternative to fossil fuels in the domain of chemical manufacturing, attaining elevated selectivity in the conversion of biomass-derived polyols while concurrently curbing CO_2 generation stand as pivotal prerequisites. This concerted endeavor facilitates the sustainable production of commodity chemicals, aligning harmoniously with environmentally conscious practices.[5]–[7]

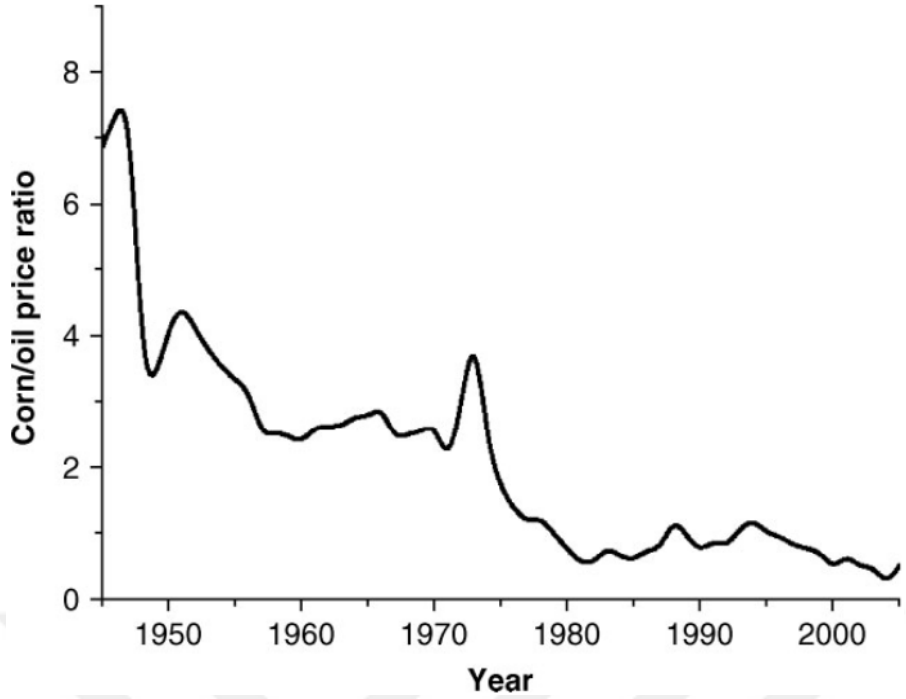

Figure 1.1. Corn (USD/Bushel)/oil (USD/Barrel) price ratio from the last of the 20th century. Adapted from Ref. [4].

1.2 Ethylene Glycol as an Alternative to Some of the Fossil Fuel Feedstocks

Ethylene glycol ($HOCH_2CH_2OH$, ethane-1,2-diol), a C_2 derivative achievable through cellulose synthesis -the latter stands as the preeminent reservoir of biomass- has garnered substantial attention due to its diverse array of applications, spanning from fuel cell utilization to the synthesis of syngas (i.e., $CO + H_2$). Positioned as the smallest constituent within the polyol category, it functions as an exploratory molecule, adept at furnishing foundational insights into the intricate interplay among C-O, C-H, C-C, and O-H bond cleavages within polyols, as elucidated by prior research.[8]–[19] Moreover, its relatively elevated vapor pressure as compared to other polyols in conjunction with its relatively modest hydrogen atom count designates it as an optimal candidate for the examination of reaction mechanisms under ultra-high vacuum (UHV) conditions.

1.3 A Literature Review on Alcohol and Ethylene Glycol Decomposition and Oxidation on Single Crystal Model Catalysts

1.3.1 Roles of Oxygen on Pd(111) Surface

Exposing oxygen to a pristine Pd(111) surface at a temperature of 100 K results in four distinct adsorption states, each characterized by varying levels of stability, as illustrated in Figure 1.2.[20] Among these states, three are associated with weakly bound molecular adsorption states, specifically identified as superoxo (α_3), Peroxo-I (α_2), and Peroxo-II (α_1) with increasing adsorption energy, respectively. Notably, the corresponding desorption temperatures for these states have been determined as 125 K, 150 K, and 200 K, respectively. These desorption peaks exhibit a clear adherence to first-order desorption kinetics. Upon employing the Readhead equation to calculate the adsorption energies, the resulting values are found as 31.8 kJ/mol, 38.1 kJ/mol, and 51.4 kJ/mol for superoxo, Peroxo-I, and Peroxo-II states, respectively.[21]

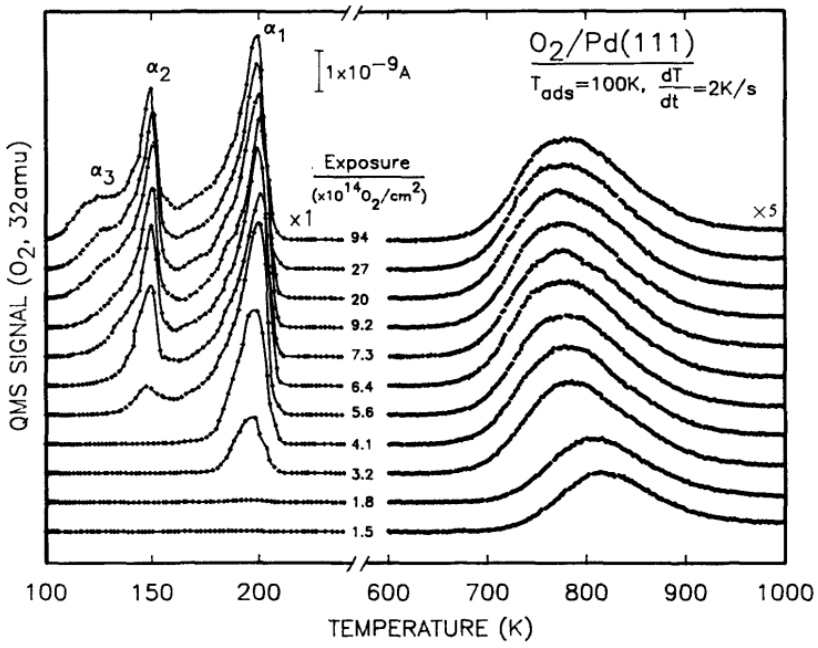

Figure 1.2. TPD spectra of oxygen on Pd(111) upon various O_2 exposures at 100 K. Adapted from Ref. [20]

Conversely, the most stable desorption state, observed approximately at a desorption maximum of 800 K, is attributed to chemisorbed atomic oxygen. The decrease in desorption temperature of this feature with increasing oxygen coverage indicates that dosed oxygen molecules dissociate on the surface leading to second order desorption kinetics. Among these four distinct states, the chemisorbed atomic oxygen state is singularly implicated as the catalytically active state due to the limited adsorption strength of the remaining molecular (unactivated) diatomic oxygen species. This pivotal distinction underscores the significance of atomic oxygen states in facilitating catalytic reactions.

Figure 1.3 illustrates the dynamic evolution of these four states across oxygen coverage. Notably, during the initial exposure to molecular oxygen, the first state to be populated is the atomic oxygen state. As coverage reaches 0.10 (O/Pd), the accumulation of the Peroxo-II (α_1) state commences, followed subsequently by the superoxo (α_3) and Peroxo-I (α_2) states. The atomic oxygen state saturates at an approximate coverage of 0.15 O/Pd. This saturation point holds particular importance as it indicates that, despite the potential for a greater oxygen presence on the surface, only the fraction corresponding to 0.15 O/Pd is likely to be potentially relevant to catalytic activity. The remaining oxygen states, while present in larger quantities, exhibit characteristics that could be less critical to the catalytic efficacy of the surface.

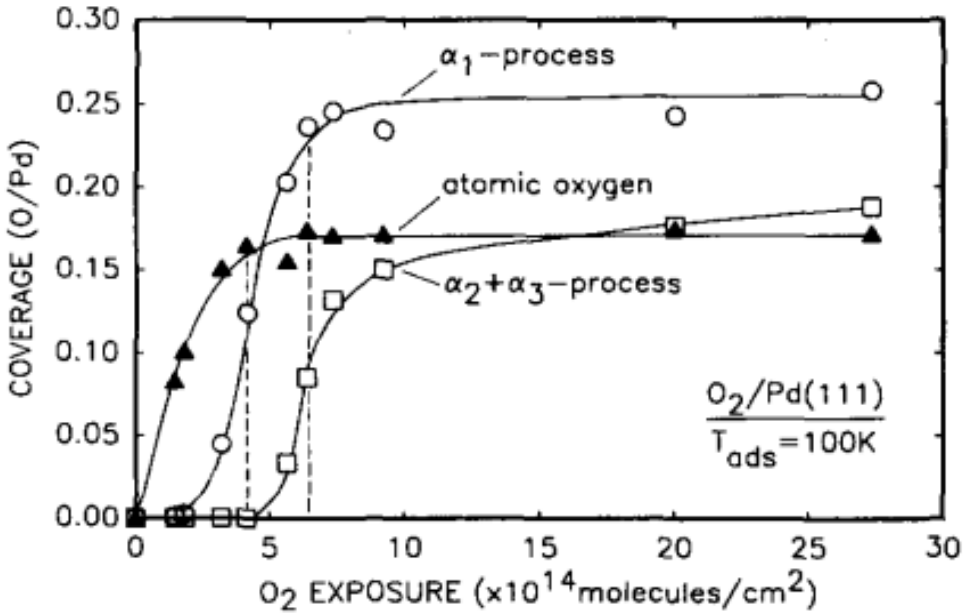

Figure 1.3. Oxygen desorption yields through different desorption processes as a function of O_2 exposure on Pd(111). The dashed lines indicate corresponding O_2 exposures for the midpoints in the yields. Adapted from Ref. [20].

Oxygen's catalytic role has been intensely studied in alcohol and aldehyde reactions on Pd(111). Some of the most prominent functionalities of oxygen species in such reactions have been reported as follows:[22], [23]

1. Proton abstraction from Brønsted acids.
2. Stabilization of adsorbed alkoxide intermediates.
3. Alteration of the adsorbed state of carbonyl compounds.
4. Oxidation of adsorbates to form surface carboxylates.
5. Scavenging of adsorbed hydrogen atoms to form water.

These effects of oxygen were elucidated in the next section.

1.3.2 Alcohol and Aldehyde Conversion on Pd(111)

The investigation of reactions involving simple alcohols and aldehydes holds a pivotal role in comprehending the decomposition and oxidation processes of polyols. Consequently,

this section summarizes the discourse surrounding the decomposition and oxidation reactions of the methanol, ethanol and formaldehyde over the Pd(111) model catalyst.

1.3.2.1 Methanol Decomposition and Oxidation on Pd(111)

As shown in Figure 1.4a, upon the saturation exposure of methanol on Pd(111) surface at 170 K, only H_2 and CO was produced at 330 K and 490 K, respectively.[22] Also, molecularly adsorbed methanol desorbed at 200 K. It is important to note that no partial dehydrogenation products such as formaldehyde or hydrocarbons were observed. The adsorption of methanol on Pd(111) occurs through lone pairs of oxygen and the activation of O-H bond, which was reported also on the Ni(111) surface.[24]

In Figure 1.4b, when methanol was exposed on Pd(111)-O(2x2) surface, which contained one quarter monolayer of oxygen atoms, 4 additional products were observed namely; formaldehyde, formic acid, carbon dioxide, and water.[25] Additionally, a second desorption peak of methanol at 230 K was also observed which was attributed to hydrogenation of surface methoxide in the light of High-Resolution Electron Energy Loss Spectroscopy (HREELS) analysis. Formaldehyde desorption at 240 K in Figure 1.4b, which has to yield through surface methoxides, further supported this claim. Formation of carbon dioxide and acetic acid was attributed to decarboxylation and hydrogenation of surface formate intermediate which was produced through the attack of surface oxygens.

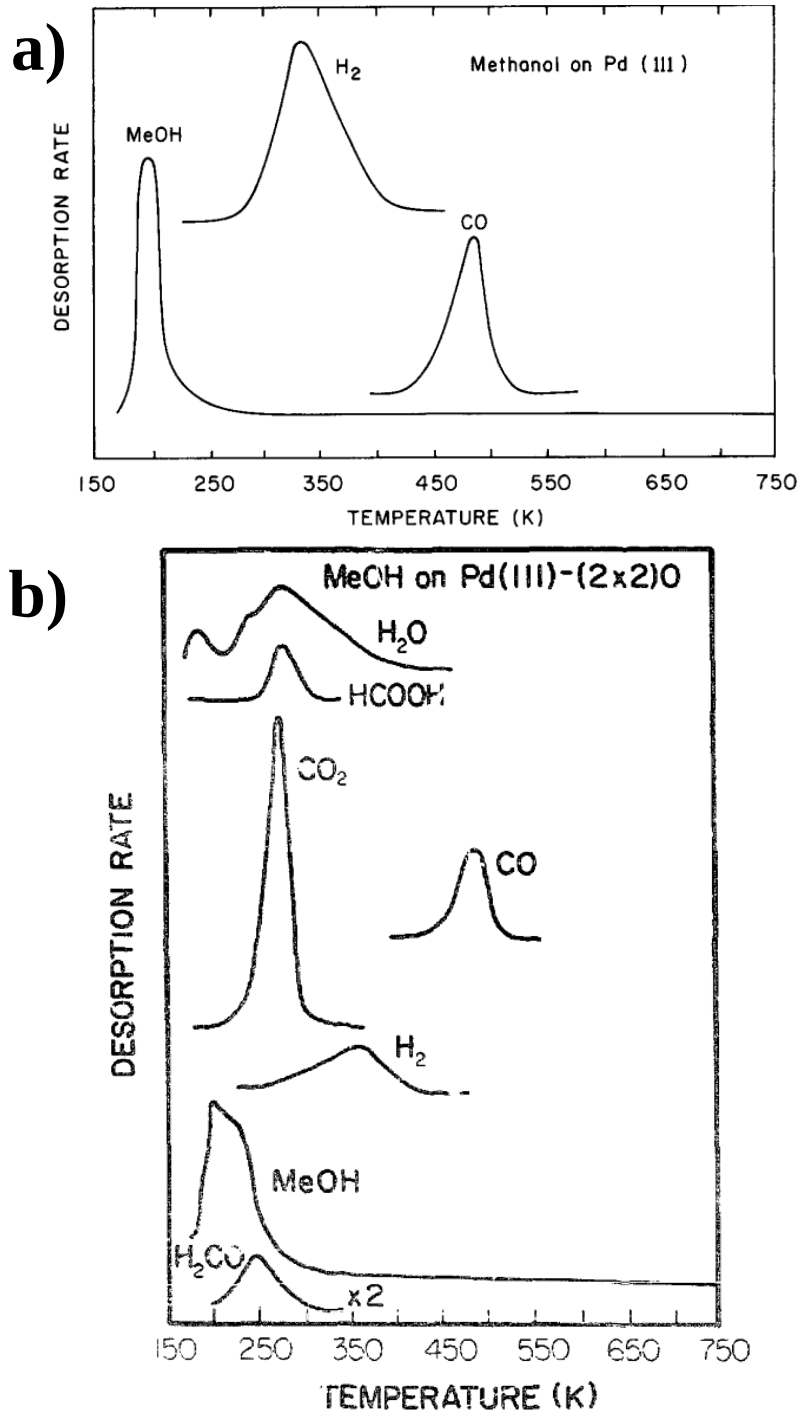

Figure 1.4. Product desorption spectra observed upon a saturation exposure of a) methanol on pristine Pd(111), b) methanol on Pd(111)-O(2x2) at 170 K. Adapted from a) Ref. [22] and b) Ref. [25]

Finally, as shown in Figure 1.4b, water formation was observed through 3 different desorption states at 190 K, 240 K, and 280 K. 190 K desorption feature was attributed to repetitive abstraction of hydrogen from the OH group of methanol by the surface oxygen

(equation 1.1). Desorption signal at 240 K was a result of OH + OH disproportionation reaction (equation 1.2), and finally 280 K signal was ascribed to the O + H reaction (equation 1.3) on the surface.[25]–[27]

$$2ROH(a) + O(a) \rightarrow 2RO + H_2O(g) \quad (1.1)$$

$$OH(a) + OH(a) \rightarrow H_2O(g) + O(a) \quad (1.2)$$

$$2H(a) + O(a) \rightarrow H_2O(g) \quad (1.3)$$

Another study on methanol oxidation over Ag(111) is specifically intriguing, as the oxidation products were related to two different types of oxygen, namely nucleophilic (O_n) and electrophilic (O_e) oxygens.[28] The effects of these two distinct oxygens on the reaction mechanism are illustrated in Figure 1.5.

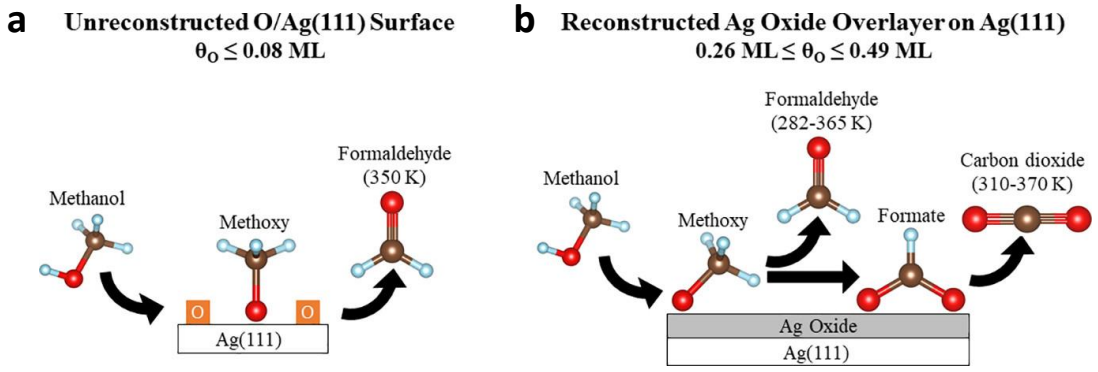

Figure 1.5. a) Electrophilic oxygen (O_e) dominates at low oxygen coverages and on unreconstructed O/Ag(111) surfaces. This configuration results in a high selectivity for formaldehyde production. b) With higher oxygen coverages, nucleophilic oxygen (O_n) becomes dominant, leading to surface reconstruction. This dominance enhances CO_2 formation and suppresses formaldehyde selectivity. Adapted from Ref. [28]

Although the electronic natures of the surface oxygens are not the primary focus of this study, the roles of oxygen atoms should not be overlooked and warrant investigation in future studies.

1.3.2.2 Ethanol Decomposition and Oxidation on Pd(111)

HREELS and isotopically labeled ethanol experiments on Pd(111) have revealed that ethanol adsorbs through its oxygen, with the initial decomposition step involving alkoxide formation due to O-H bond cleavage.[29] The rate-limiting step was suggested to be the scission of the C^{α}-H bond [30] Alkoxide formation via O-H bond activation has also been observed on Ag(110), Cu(110), and Ni(111).[31], [32] Figure 1.6 illustrates the desorbed products—methane, hydrogen molecules, carbon monoxide, and unreacted ethanol—resulting from the adsorption of ethanol at 170 K on clean Pd(111).[22]

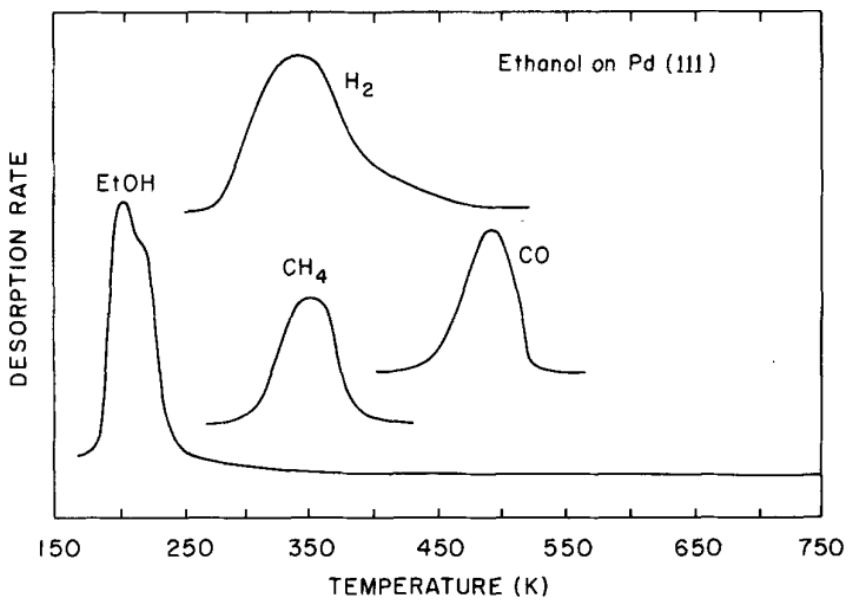

Figure 1.6. Product desorption spectra observed upon a saturation exposure of ethanol on pristine Pd(111) at 170 K. Adapted from Ref. [22]

Similar to the case of methanol adsorption/desorption on Pd(111), there has been no observation of partial dehydrogenation products when ethanol was adsorbed on pristine Pd(111) as indicated on Figure 1.6. Furthermore, the Pd(111) surface facilitates the activation of the C-O bond, resulting in methane formation. This phenomenon was not observed when ethanol was dosed on a pristine Rh(111) surface, indicating that Rh(111) prefers C-C bond scission over C-

O bond cleavage.[33] The following reaction sequence was proposed for the decomposition of methanol, ethanol, and 1-propanol on the pristine Pd(111) surface; [22]

$$RCH_2OH(g) \rightarrow RCH_2OH(a) \quad (1.4)$$

$$RCH_2OH(a) \rightarrow RCH_2OH(g) \quad (1.5)$$

$$RCH_2OH(g) \rightarrow RCH_2O(a) + H(a) \quad (1.6)$$

$$RCH_2O(g) \rightarrow RCHO(a)\,\{\eta^2(O,C)\} + H(a) \quad (1.7)$$

$$RCHO(a)\,\{\eta^2(O,C)\} \rightarrow R(a) + CO(a) + H(a) \quad (1.8)$$

Theoretical calculations on the Rh(111) surface have likewise confirmed similar reaction steps. Figure 1.7 illustrates the decomposition steps of ethanol, along with the dehydrogenation steps of the beta carbon, on the Rh(111) surface. [34] According to these calculations, the activation energies of both the C-C and C^{β}-H bonds decrease as the dehydrogenation process begins.

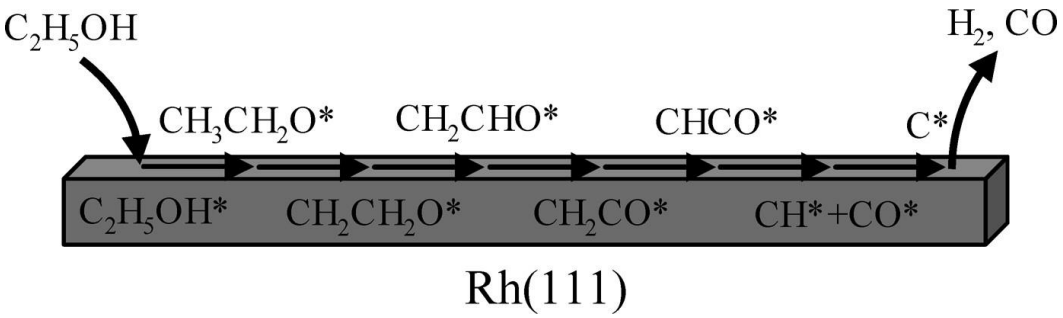

Figure 1.7. The decomposition steps of ethanol on Rh(111). The most stable intermediates were determined using Density Functional Theory (DFT). Adapted from Ref. [34]

In Figure 1.8, upon ethanol adsorption on Pd(111)-O(2x2), a distinct reaction pathway emerged, resulting in the formation of acetaldehyde (CH_3CHO), acetic acid (CH_3COOH), and

carbon dioxide.[25] These products were also observed when ethanol was adsorbed on oxidized Rh(100) surfaces.[26] The formation of CO_2 and H_2O was favored under oxygen-rich conditions, while under oxygen-lean conditions, methane formation was enhanced for both Pd(111) and Rh(100). Remarkably, apart from acetaldehyde, the origin of these products was traced back to acetate intermediates residing on the Pd(111)-(2x2)O surface.[25], [29] The hydrogenation of acetate led to acetic acid, while its decarboxylation gave rise to carbon dioxide and water.

It is essential to emphasize that one may anticipate the formation of hydrocarbons through decarboxylation of surface acetates on Pd(111)-O(2x2) surface. However, on this surface, intriguingly, no hydrocarbons were observed above 400 K. This absence indicates that the methoxy group ($-CH_3$) of the acetate remained on the surface and decomposed to surface hydrogen (H_{ads}) and carbon (C_{ads}). This interpretation gains further support from the observed tail in carbon monoxide desorption above 500 K, which signifies the reaction between oxygen and surface carbon. The following reaction sequence was proposed for the decomposition of methanol, ethanol and also 1-propanol on Pd(111)-(2x2)O surface; (note that water formation steps are not included here, as they were previously presented in equations 1.1-1.3.)

$$RCH_2OH(a) \rightarrow RCH_2O(a) + H(a) \tag{1.9}$$

$$RCH_2O(a) \rightarrow \eta^1 - RCHO(a) + H(a) \tag{1.10}$$

$$\eta^1 - RCHO(a) \rightarrow RCHO(g) \tag{1.11}$$

$$\eta^1 - RCHO(a) + O(a) \rightarrow RHCO_2(a) \tag{1.12}$$

$$RHCO_2(a) \rightarrow RCO_2(a) + H(a) \tag{1.13}$$

This reaction scheme is also applicable to some of the Group VIII catalytic metals such as Ru, Pt, Ni and Rh.[32], [33], [35], [36]

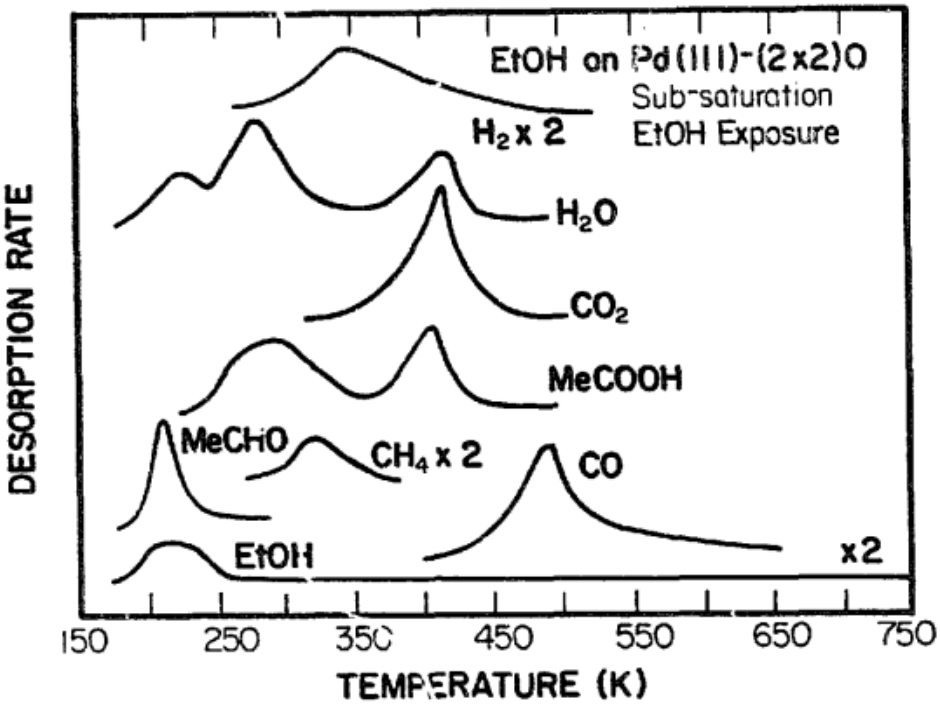

Figure 1.8. Product desorption spectra observed upon a saturation exposure of ethanol on Pd(111)-O(2x2) at 170 K. Adapted from Ref. [25]

It is noteworthy that in both the methanol and ethanol oxidation reactions on Pd(111), all five roles of oxygen have been identified.[25] Initially, the abstraction of a proton from Brønsted acids to generate OH groups, which subsequently participate in a disproportionation reaction leading to the formation of water, were prominently observed.[25], [31] Following this, a direct abstraction of surface hydrogen atoms to produce water molecules was reported. The stabilization of alkoxy intermediates, accompanied by alterations in adsorption configurations on the surface, was also discernible through their elevated desorption temperatures in the case of oxidized Pd(111) surfaces.[29] Lastly, the creation of surface carboxylates, specifically in the form of formic acid and acetic acid, has been verified.

1.3.3 Decomposition and Oxidation of Formaldehyde on Pd(111)

Upon exposure of formaldehyde on pristine Pd(111) surface at 170 K, formaldehyde was found to decompose to CO and H_2 at 170 K, as illustrated in Figure 1.9.[37] These products desorbed from the surface at 470 K and 300 K, respectively. Being different from simple alcohols, formaldehyde also polymerized on the surface to produce paraformaldehyde $(H_2CO)_n$ as supported by HREELS data.[29], [37] Hence, formaldehyde desorption at 260 K, as seen in Figure 1.9, was not attributed to molecularly adsorbed formaldehyde but rather to the decomposition of paraformaldehyde. The paraformaldehyde formation was not observed on pristine Rh(111) surface where adsorbed formaldehyde desorbed and decomposed between 90 – 140 K.[38] Compared to production of formaldehyde via methanol oxidation on Pd(111), the desorption signal at 260 K upon formaldehyde adsorption on Pd(111) was 15 K higher; offering further evidence of paraformaldehyde stabilization and subsequent controlled decomposition on clean Pd(111). Moreover, HREELS results indicated that paraformaldehyde desorption intensity decreased between 240 and 260 K, whereas CO intensity increased.[29], [37] Thus, most of the paraformaldehyde went into decomposition to form CO and H_2 on clean Pd(111), limiting the molecular formaldehyde desorption.

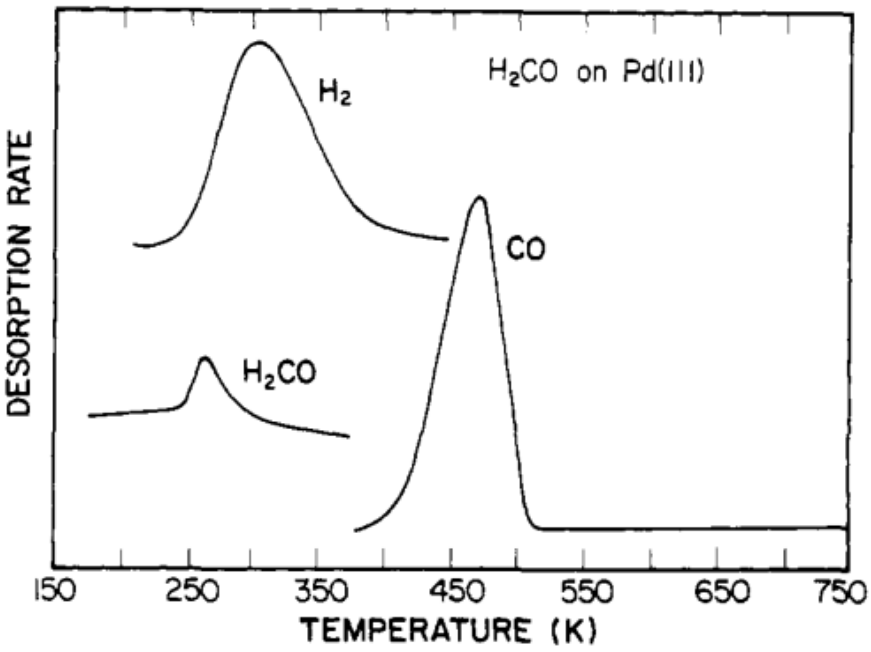

Figure 1.9. TPD spectra observed upon a saturation exposure of H_2CO on the clean Pd(111) surface at 170 K. Adapted from Ref. [37]

Exposing formaldehyde to the Pd(111)-(2x2)O surface at 170 K resulted in the formation of CO_2, formic acid (HCOOH), water, as well as formaldehyde, hydrogen and CO.[39] TPD spectra illustrating such reaction products are presented in Figure 1.10. It has been asserted that the oxidation of formaldehyde occurs via dioxymethylene ($-OCH_2O-$) intermediates, which have also been observed on Ag(110) and Cu(110) surfaces.[40]–[42] This transitory and unstable surface intermediate was reported to subsequently undergo two competing reactions. These reactions involved the initiation of formaldehyde polymerization leading to paraformaldehyde generation, and the dehydrogenation process yielding surface formates.

Being similar to aldehyde adsorption on pristine Pd(111), as shown in Figure 1.9 previously, the decomposition of paraformaldehyde was also discerned at approximately 260 K on the Pd(111)-O(2x2) surface (Figure 1.10).[37], [39] However, on the Pd(111)-O(2x2) surface, the desorption intensity of H_2CO was notably greater. This suggested the influence of oxygen in either fostering a greater extent of polymerization towards paraformaldehyde or enhancing the

selectivity of paraformaldehyde decomposition into formaldehyde, as opposed to CO and H_2 formation on the Pd(111)-O(2x2) surface.[39] On Rh(111)-O(2x2) surfaces, the formation of paraformaldehyde was observed, a phenomenon not evident on clean Rh(111). Moreover, all paraformaldehyde present decomposed into formaldehyde monomers, carbon monoxide, carbon dioxide, and hydrogen. This observation reinforces the notion that surface oxygen atoms contribute to paraformaldehyde formation. [38] However, investigations on both Ag(110) and Pd(111) surfaces have supported the argument that formyl intermediates play a role in paraformaldehyde formation on these surfaces. [29], [37], [40] Hence, the main role of oxygen on Rh(111)- O(2x2) surface could be associated with the formation of surface formyl which ultimately starts the polymerization reaction.

Figure 1.10 also depicts the desorption of CO_2 and formic acid (HCOOH) from Pd(111)-O(2x2) at 270 K. The emergence of these products signifies the existence of formate ($HCOO^-$) species on the surface. These surface formates can follow two distinct paths: either undergoing decarboxylation reactions resulting in the formation of CO_2 and surface hydrogen, or engaging in hydrogen transfer from the surface to form acetic acid. Ultimately, the intensities of desorbed products originating from both formate ($HCOO^-$) and formaldehyde (H_2CO) sources are contingent upon the relative rates of polymerization versus dehydrogenation of dioxymethylene ($H_2CO_2^-$) species. The water peak observed at 200 K in Figure 1.10 was attributed to the dehydrogenation of dioxymethylene species and the direct transfer of hydrogen to surface oxygens.[39] Meanwhile, the peak observed at 260 K was attributed to the recombination of adsorbed hydrogen and oxygen atoms on the Pd(111) surface, paralleling the oxidation reactions observed in the cases of methanol and ethanol on Pd(111).[25]

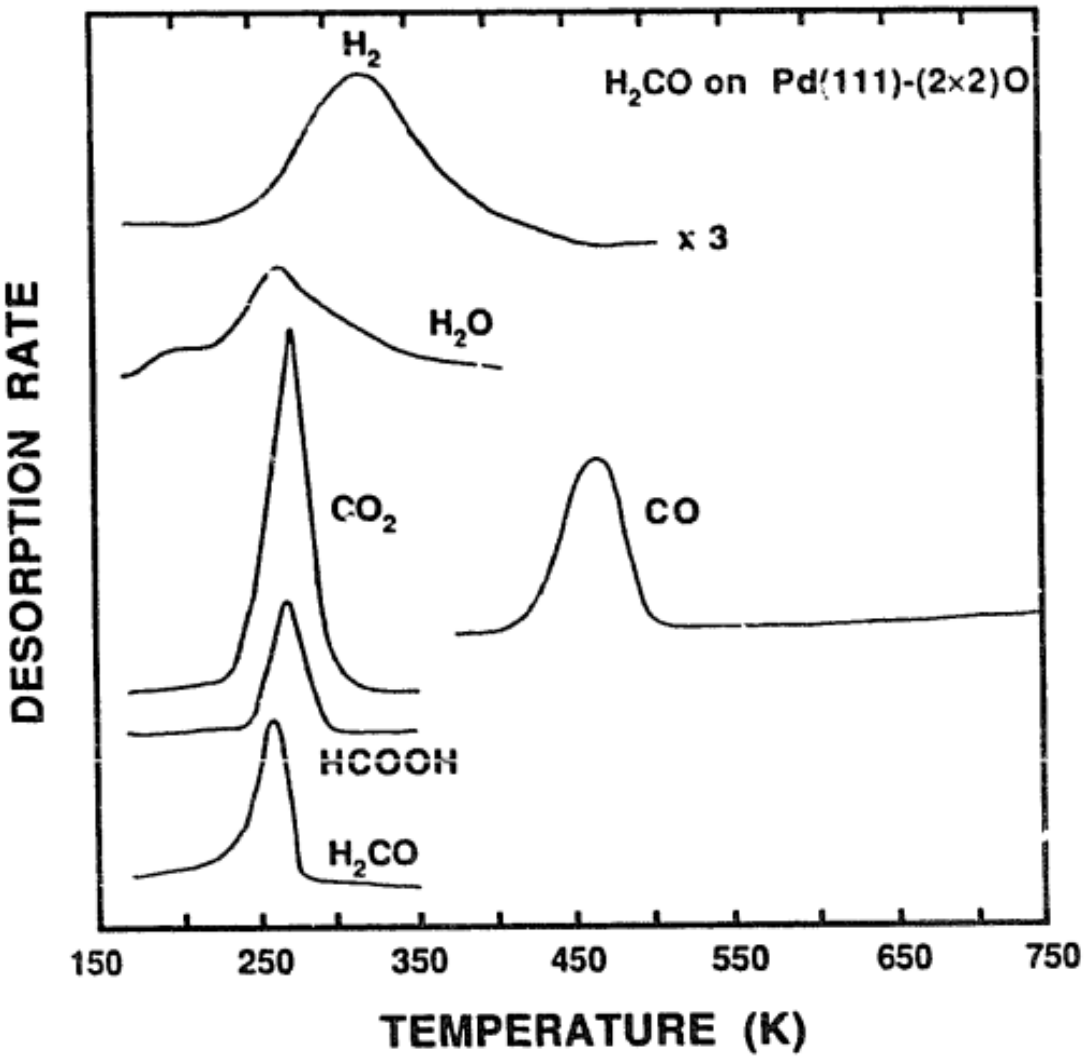

Figure 1.10 TPD spectra for the reaction of H_2CO on the pre-dosed Pd(111)-O(2x2) surface. Adapted from Ref. [39]

1.3.4 Ethylene Glycol Conversion on Single Crystal Catalysts

The investigation into the decomposition reaction of ethylene glycol has been an extensively explored subject in the past. Interaction between ethylene glycol and surfaces may primarily occur through its oxygen atoms, ultimately giving rise to the formation of ethylenedioxy (-OCH_2CH_2O-) as a result of the O-H bond cleavage. This phenomenon has been observed on a variety of pristine single crystal surfaces, including Pt(111), Ni(100), Rh(100), Rh(111), Cu(110), Mo(110), and Pd(111).[43]–[49] In scenarios involving higher surface

coverages, ethylene glycol exhibited an additional mode of binding known as monodentate binding, which was reported on surfaces like clean Rh(100) and Mo(110).[45], [50] Despite the existence of the C-O bond cleavage, albeit with limited yields of ethylene and water, a prevalent trend among most of these surfaces was the preferential scission of the C-H bond.[16], [44], [47], [49] This scission led to the production of glyoxal (-OCHCHO-), which subsequently underwent further decomposition into mainly H_2 and CO. A distinctive feature arose from the adsorption of ethylene glycol on clean Mo(110), which prominently favored the C-O bond cleavage pathway, with an outstanding 85% selectivity attributed to the robust Mo-O interaction.[50] On the contrary, pristine Ag(110) surface displayed inertness towards the decomposition of ethylene glycol.[51]

Specific to Pd(111) surface, a previous study on ethylene glycol decomposition have shown the major products indicated in Figure 1.11. [49]

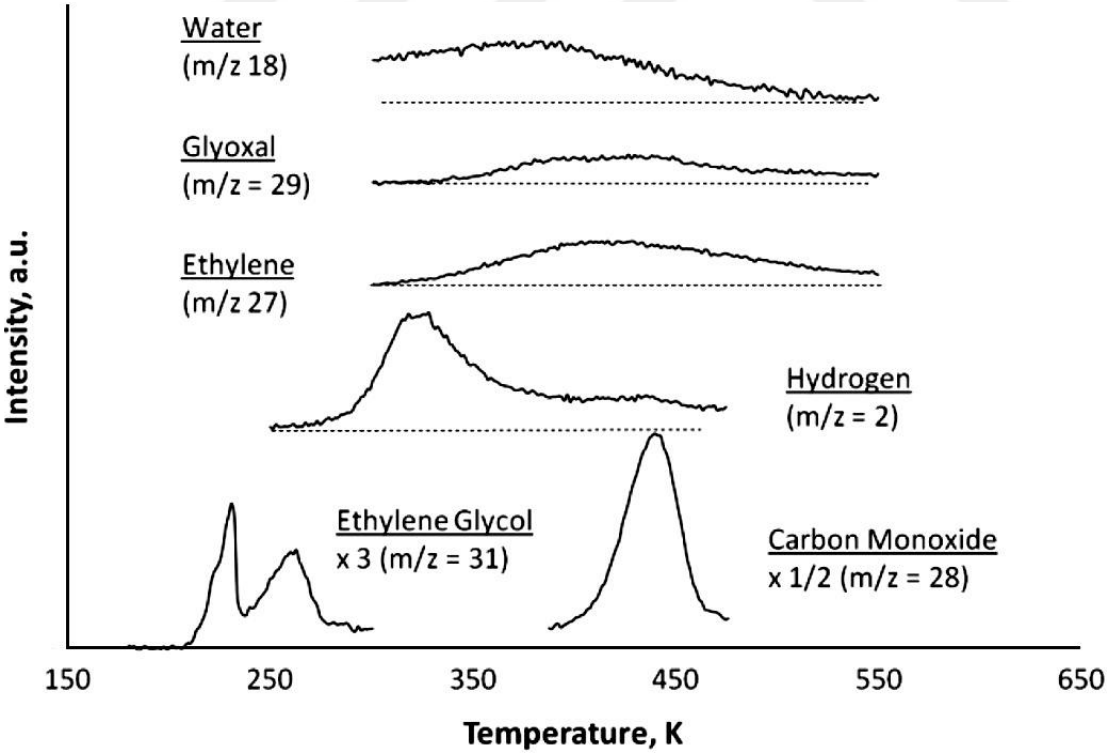

Figure 1.11. Major TPD traces from ethylene glycol dosed onto Pd(111) at 173 K. Adapted from Ref. [49].

It is illustrated in Figure 1.8 that upon adsorption of ethylene glycol on Pd(111) at 140 K, it readily underwent O-H bond activation, resulting in the formation of ethylenedioxy (-OCH_2CH_2O-).[49] Further annealing of the surface to 170 K induced dehydrogenation of C-H bonds and led to the formation of glyoxal (-OCHCHO-), which began desorbing from the surface within the temperature range of 330 K to 470 K. Increasing the temperature above 190 K also promoted decarbonylation and dehydrogenation of glyoxal, resulting in the formation of carbon monoxide and hydrogen. While the cleavage of C-O bonds in glyoxal was limited, it produced small amount of ethylene. The schematic representation of these intermediates and products are summarized in Figure 1.12.

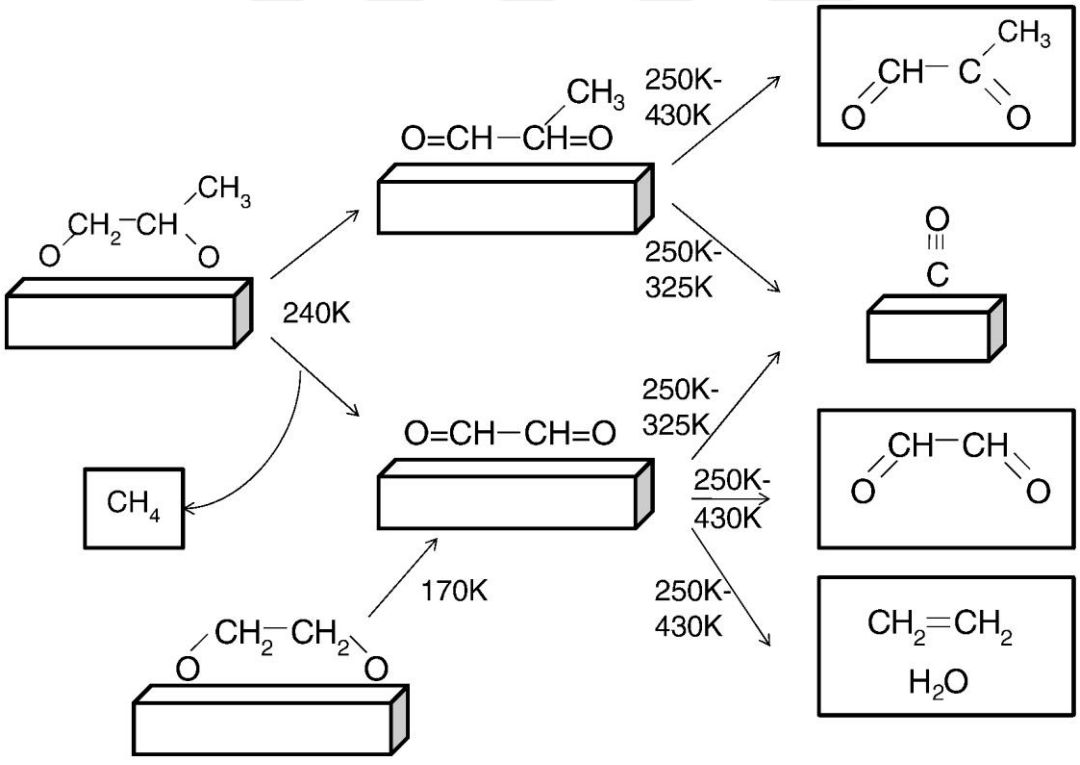

Figure 1.12. A proposed reaction mechanism of ethanedioxy and 1,2-propanedioxy on Pd(111). Adapted from Ref. [49]

Given the pivotal significance of the bond-breaking sequence in ethylene glycol reactions on single crystal surfaces, a series of theoretical calculations have been recently undertaken on both Pt(111) and Pt(211) surfaces.[52] These calculations indicated that OH bond activation was less favored than C-H bond activation so that first C-H bond cleavage occurred, which completely contradicted with the experimental results. Similar inconsistencies have been reported in other theoretical studies, as seen in the case of ethanol decomposition. In these studies, the activation energy for O-H bond activation was considered to be less likely compared to C-H bond activation upon the initial adsorption of ethanol.[53] However, it is noteworthy that all experimental studies on ethanol assert the contrary.[30]–[33] While theoretical studies yield differing initial step outcomes, their assumptions play a crucial role, especially in contexts involving C-C bond breaking sequences, which are intricate to deduce from experimental investigations.

In Figure 1.13, the most stable intermediates subsequent to the most probable C-H or O-H bond cleavages were illustrated for both Pt(111) and Pt(211) surfaces. Although the outcomes of these calculations reveal that O-H bond breakage was less likely compared to C-H bond activation upon the first adsorption of ethylene glycol which completely contradicted with the experimental results; the findings on the following dehydrogenation steps could be considered noteworthy. Based on this theoretical study, it has been ascertained that the initial dehydrogenation steps of ethylene glycol on both Pt(111) and Pt(211) were exothermic in nature; however, they were followed by endothermic steps after several dehydrogenation events.[52] Moreover, with each subsequent dehydrogenation, the likelihood of C-C bond breakage increased.

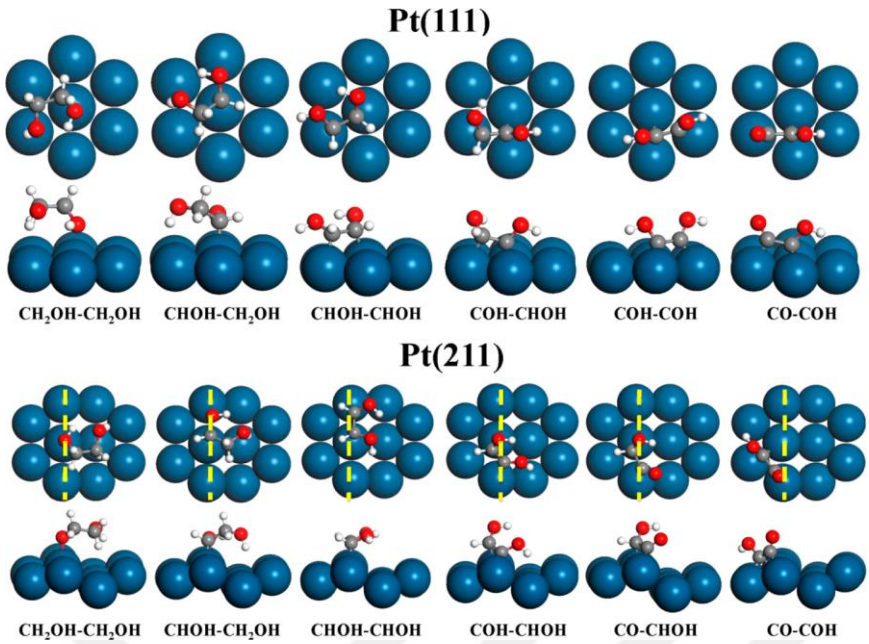

Figure 1.13. Optimized computed geometries of the most stable intermediates, at each level of dehydrogenation, involved in ethylene glycol dehydrogenation on Pt(111) and Pt(211). The blue, gray, red and white spheres represent Pt, C, O and H atoms, respectively. The dashed yellow line represents the step of Pt(211). Adapted from Ref. [52]

1.4 Motivation of the Current Study

Although extensive research has been conducted to understand the reaction pathways of ethylene glycol decomposition on atomically well-defined single crystal model catalysts under UHV conditions, limited attention has been given to its oxidation reactions, which have only been studied on Ag(110) to the best of our knowledge.[51], [54] It is important to note that Ag is one of the most utilized catalyst in the industry for partial oxidation reactions. For example, it has been reported that 10 million metric tons of methanol, which constitutes 1/3 annual methanol production, are converted to formaldehyde through the utilization of Ag catalysts.[55] Although this reaction is facile, new and more cost-effective methodologies must be investigated.

Given the increasing importance of utilizing biomass-derived sources for the production of value-added chemicals, it is crucial to gain a comprehensive understanding of the oxidation reaction mechanism of ethylene glycol on different catalysts.

Hence, in this study, we investigate the partial oxidation of ethylene glycol on a Pd(111) single crystal. Our study revealed that the main oxidation products were CO_2 and formaldehyde. Evolution of formaldehyde is proposed to be through the nucleophilic attack of surface oxygen atoms to second carbon of the -OCH_2CH_nO- *($n \leq 2$)* surface species leading to C-C bond scission. Drawing from earlier theoretical calculations, the activation energy of C-C bonds was suggested to decrease as the number of hydrogens on the second carbon decreased *(n)*. This led to two distinct formaldehyde desorption peaks at 200 and 220 K, attributed to C-C bond scission of -OCH_2CO- and -OCH_2CHO-, respectively. In these cases, the second carbons, when they react with oxygen, can form either CO_2 or surface formate, where the latter subsequently decomposed into CO_2 and surface hydrogen. On the other hand, surface species that possess at most one hydrogen on the carbons, denoted as -OCH_nCH_nO- *($n \leq 1$)*, play a role in the formation of CO, H_2, and CO_2. The inability of these intermediates to generate formaldehyde via the hydrogenation of formyl groups was demonstrated by isotopically-labeled (i.e., deuterated) ethylene glycol (DO-CD_2-CD_2-OD) TPD experiments.

Additionally, selectivity of the reaction was affected by the oxygen-to-ethylene glycol ratio (EG/O), where an excess of oxygen led to enhancement of CO_2 generation. Conversely, increasing the EG/O ratio led to the enhancement of formaldehyde production and exceeding a certain EG/O ratio resulted in the surface poisoning by ethylene glycol. Ultimately, our results suggest that fine-tuning the ethylene-glycol to oxygen ratio without poisoning the surface of Pd(111) was essential for the production of valuable products.

Chapter 2

2 Experimental

2.1 Experimental Setup

Experiments were conducted using a custom-design multifunctional UHV surface analysis system, as illustrated in Figure 2.1. The UHV conditions were achieved through the utilization of a turbomolecular pump (Varian, TV 551 Navigator), with a pumping speed of 550 L/s, in conjunction with an oil-free scroll pump (Agilent Varian SH-110). Augmenting the setup, a titanium sublimation pump (TSP) (Varian, Model 916-0017) was employed to eliminate highly diffusive gases characterized by low compression factors, such as H_2 and CO, as well as adhesive gases like H_2O. Throughout the experiments, a base pressure of 5×10^{-11} Torr was maintained.

The custom-design UHV chamber used in the current study featured an array of surface-sensitive characterization instrumentation, encompassing a Low Energy Electron Diffraction (LEED) setup, Temperature Programmed Desorption (TPD) apparatus, a custom-designed Infrared Reflection Absorption Spectroscopy (IRAS) setup, the X-ray Photoemission Spectrometer (XPS), and an Ar^+ sputtering ion gun (LK technologies, NGI3000, 1.5 kV x 15 mA) primarily deployed for cleansing of the Pd(111) single crystal surface.

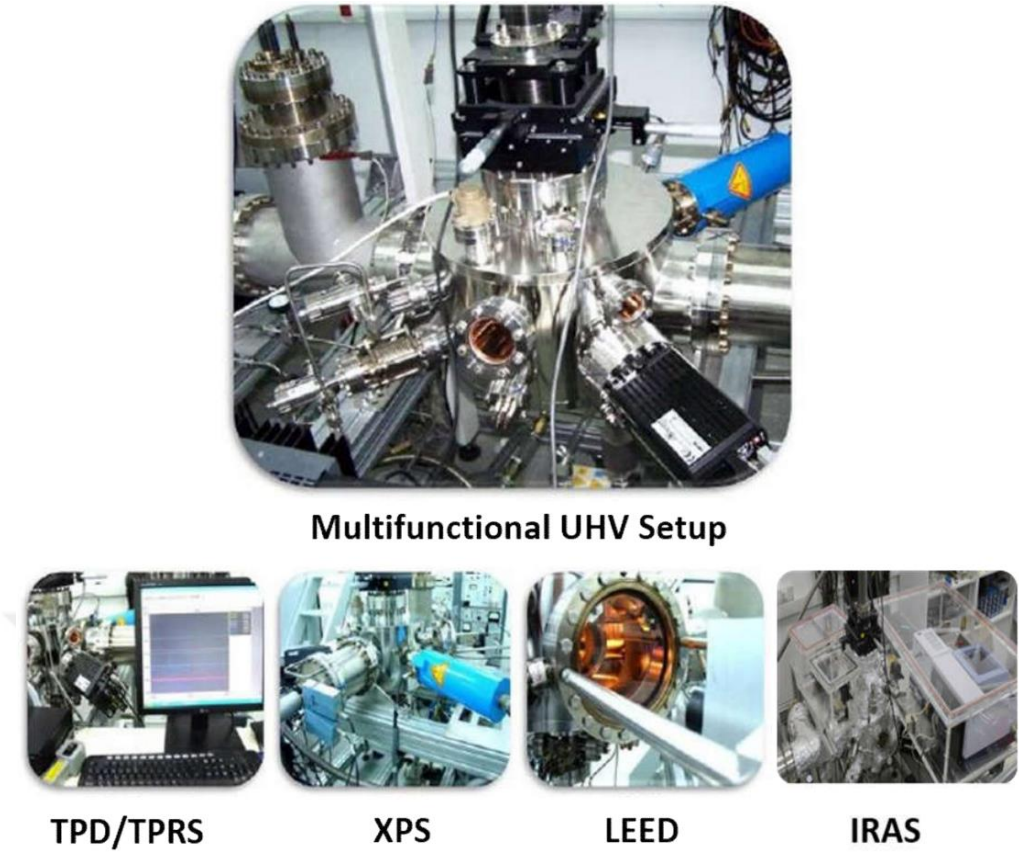

Figure 2.1. Various sub-components of the custom design multi-functional UHV chamber utilized in the current work.

A Pd(111) single crystal, a disc with a 10 mm diameter and 1 mm thickness, meticulously polished on both sides, with a purity surpassing 99.999% sourced from MaTeck GmbH, was securely affixed to Ta wires. This setup facilitated efficient sample cooling to 90 K through liquid nitrogen, while also enabling sample heating to 1000 K via resistive heating. The temperature of the sample was measured using a K-type thermocouple (thickness: 0.005 in., Omega Inc.), spot-welded onto the upper facet of the Pd(111) disc. Additionally, introduction of gaseous reactants into the chamber was done via three distinct high-precision all metal leak valves, ensuring a controlled and reproducible dosing process.

2.2 Temperature Programmed Desorption/Reaction Spectroscopy (TPD/TPRS)

In this study, primarily the TPD technique was employed to quantify the products and analyze the mechanistic insights arising from decomposition and oxidation of ethylene glycol. Basics of the TPD technique are elucidated in the subsequent section.

2.2.1 Fundamentals of the TPD Technique

This study utilized an Ametek Dycor Dymaxion DM200 Quadrupole Mass Spectrometer (QMS), shown in Figure 2.2a, equipped with an apertured (differentially pumped) shield, in conjunction with a sample heater regulated by a Proportional-Integral-Derivative (PID) controller. All TPD experiments were executed using a constant heating rate of 1 K/s, the QMS ionization energy of 70 eV, and a dwell time of 30-120 ms for each desorption channel.

TPD is a characterization technique that enables the differentiation of desorbing products through the utilization of a QMS. In this technique, reactants are dosed on the model catalyst surface under UHV conditions at typically cryogenic temperatures (i.e., $T \geq 77$ K). The crystal is then brought in front of the QMS, and is heated linearly with time, leading to the activation of various desorption and/or reaction channels available to the adsorbates. The resulting products desorb from the surface based on their characteristic activation energies for formation or desorption. Multiple products can be simultaneously monitored – up to eight separate desorption channels in our study -enabling the entire reaction to be deciphered. When combined with isotopic labeling, this method may uncover additional mechanistic insights into the bond ruptures of a catalytic conversion reactions. It can also be complemented by spectroscopic techniques such as photoelectron or vibrational spectroscopies.[56]–[58]

During desorption of the products, a current is directed through the QMS ionizer filament, promoting the thermionic emission of electrons. These electrons are then accelerated towards the ionization chamber, inducing electron impact ionization and conferring a positive charge upon the products. As shown in Figure 2.2b, the positively charged species traverse through the quadrupole heads of the QMS, which selectively identifies these entities based on their mass-to-charge ratios, achieved through continuous alterations of the electric field. Ultimately, these charged molecules impinge upon the detector, generating a measurable cationic current that facilitates the real-time monitoring of the desorption events.

Consequently, the desorption intensity over time, later converted to temperature, is plotted to generate a TPD profile. This TPD profile provides valuable insights into the desorption process and contributes to a deeper understanding of the studied surface reaction.

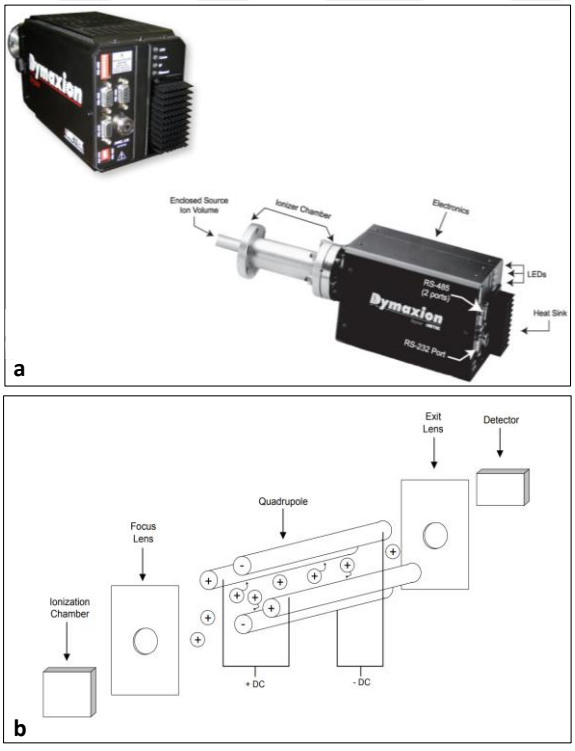

Figure 2.2. a) Ametek Dycor Dymaxion DM200 Quadruple mass spectrometer (QMS) used in this study. b) Internal parts of the QMS. Adapted from Ref. [59]

2.2.2 Analysis of TPD Spectrum

The desorption characteristics in a TPD experiment can be quantitatively described by applying the Polanyi-Wigner equation[56], as presented in Equation 2.3.

$$r = -\frac{d\theta}{dT} = k_{des}\theta^m \tag{2.1}$$

$$T = T_0 + \beta t, \qquad \beta = \frac{dT}{dt} \tag{2.2}$$

$$r = -\frac{d\theta}{dT} = \frac{k_{des}}{\beta}\theta^m = -\frac{d\theta}{dt} = k_{des}\theta^m = A\theta^m e^{\left(\frac{E_{des}}{RT}\right)} \tag{2.3}$$

Equation 2.3 describes the desorption behavior in terms of various parameters: r represents the desorption rate, θ corresponds to the adsorbate coverage, m indicates the order of desorption, t denotes time, k_{des} is the rate constant of desorption, A is the pre-exponential factor, E_{des} signifies the desorption energy, R represents the universal gas constant, T signifies temperature, T_0 is the initial adsorption temperature and β is the linear heating rate. According to Equation 2.3, desorption only occurs above a certain temperature threshold, as the magnitude of E_{des} must be exceeded at these specific temperatures. [56]

Polanyi-Wigner equation also predicts that adsorbates with different desorption orders (m) will have distinct desorption shapes. Figure 2.3a presents three prevalent desorption orders along with their corresponding curves. In instances of zeroth-order desorption ($m = 0$), the desorption rate remains unaffected by adsorbate coverage. This behavior is generally observed when excess adsorbate desorbs from the surface, as seen in multilayer desorption scenarios. Moreover, the leading-edge profile of the TPD spectra for zeroth-order desorption remains intact as coverage increases, while the desorption maxima increases with increasing adsorbate coverage.

First-order desorption kinetics ($m = 1$) manifest when molecular (i.e., non-dissociative) adsorption and desorption occurs, exemplified by the adsorption of CO_2 on Pd(111).[60] As displayed in Figure 2.3b, first-order desorption peaks exhibit a specific asymmetry, and the desorption temperature remains unchanged with increasing adsorbate coverage. In the context of layer-by-layer growth, the saturation point of the desorption signals obeying first order kinetics serves as a reference point for determining 1 (i.e., the first) monolayer (ML) and quantifying the adsorbate coverage in subsequent TPD profiles.

Conversely, second-order desorption kinetics ($m = 2$), shown in Figure 2.3c is observed when the desorption rate is proportional to the square of the adsorbate coverage. This behavior emerges due to the recombinative desorption of molecules which are initially adsorbed in a dissociative manner on the surface, such as H_2 on Pd(111).[61] Consequently, the desorption temperature linked to this type of kinetics decreases as adsorbate coverage increases, attributable to more facile recombination at higher coverages.

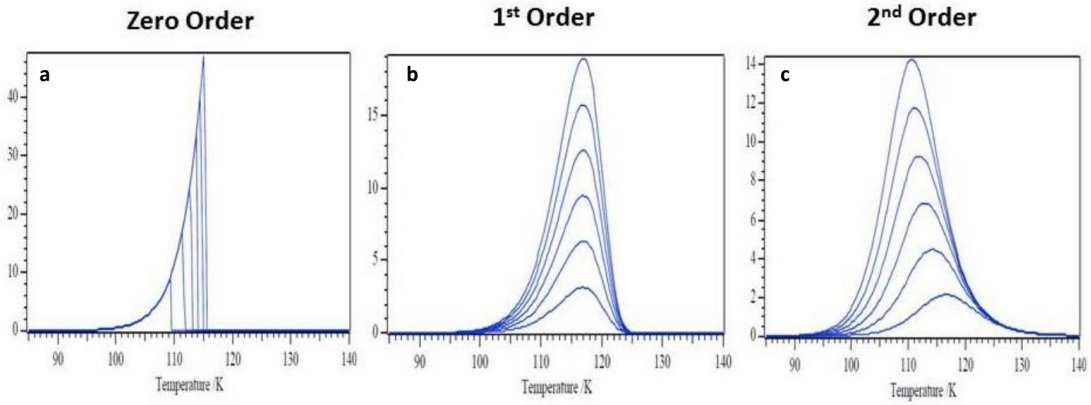

Figure 2.3. a) Sample TPD spectra obtained for a) zeroth order, b) first order, c) second order desorption kinetics as a function of increasing adsorbate coverage. Adapted from Ref. [56], [62]

2.2.2.1 Readhead Analysis

Readhead Analysis can be applied to calculate the adsorption energy of an adsorbate exhibiting first-order desorption kinetics ($m = 1$). The Readhead equation[21], presented as Equation 2.4, is utilized for this purpose.

$$E_{des} = RT_m(\ln\frac{AT_m}{\beta} - 3.46) \tag{2.4}$$

Where T_m represents the desorption peak's maximum temperature, and the ratio $\frac{A}{\beta}$ provides insights into the statistical density of microstates. It is worth noting that as the number of available microstates increases, the desorption process becomes more favorable. Typically, this ratio is maintained within the range of $10^8 - 10^{13}\ K^{-1}$, as the desorption transition state strikes a balance between being neither excessively constrained nor overly relaxed, resulting in a moderate level of statistical density of microstates. [56]

2.2.2.2 Leading Edge Analysis

Leading edge analysis constitutes a second method for acquiring insights into desorption kinetics and thermodynamics. In this approach, a linear segment of the TPD curve situated in the vicinity of the peak take-off region is leveraged to determine the desorption energy of an adsorbate. By employing data points corresponding to this linear portion of the TPD curve, a ln(r) vs 1/T curve is constructed, from which the desorption energy is derived via the slope. [56]

It is noteworthy that while leading edge analysis entails a smaller number of assumptions and approximations compared to Redhead Analysis, the former method is utilized less frequently. This is primarily due to the prerequisite of TPD profiles for the leading edge analysis possessing a very high signal-to-noise ratio to attain precise numerical outcomes.

2.3 Experimental Procedures

2.3.1 Cleaning of Pd(111) Single Crystal Model Catalyst

It is well-known that the most prominent contamination sources on Pd(111) single crystal surfaces under UHV conditions are C, O, H atoms as well as other species containing these three atoms, most prominently CO. Adsorbed H on the Pd(111) surface can be readily removed via annealing in UHV. Then the remaining amounts of surface C and O can be quantitatively analyzed with the help of monitoring CO (m/z = 28) desorption in TPD. Figure 2.4a shows our CO-TPD results for the Pd(111) surface after our cleaning procedure (which will be described in detail below) as well as CO-TPD obtained upon increasing additional coverages (1 Langmuir (L) = 10^{-6} Torr.s) of CO introduced on the clean Pd(111) at 88 K. Compared to the literature, residual (background) CO coverage on our clean Pd(111) surface lies below the 0.01 ML, demonstrating the successful cleaning of the Pd(111) single crystal model catalyst after the currently utilized surface cleaning procedures .[63]

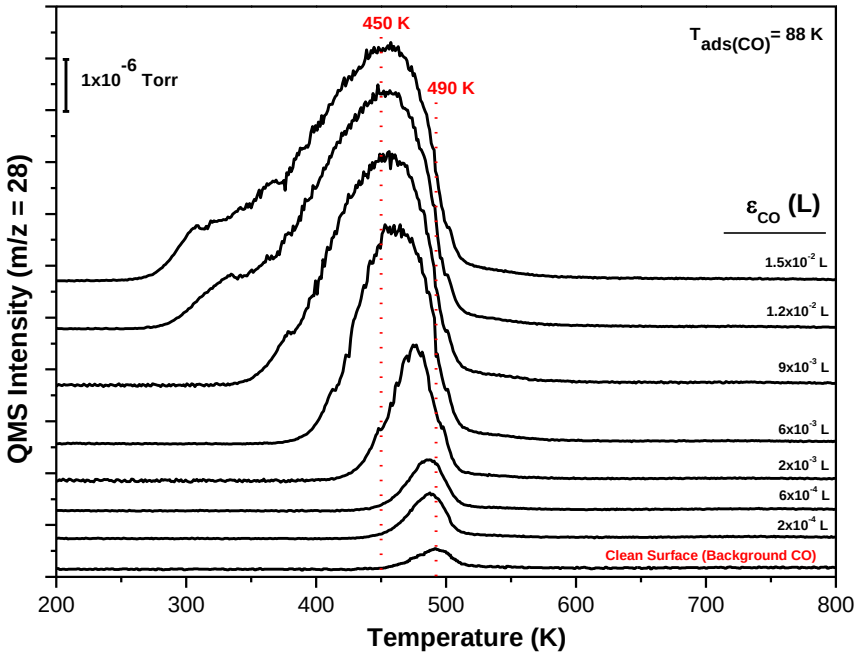

Figure 2.4. m/z = 28 TPD spectra for the clean Pd(11) surface and increasing CO exposures on Pd(111).

To achieve such surface cleanliness, two distinct cleaning methodologies were employed.

2.3.1.1 Surface Cleaning via Ar^+ Sputtering

To facilitate surface cleaning of Pd(111), an ion gun (RBD instruments IG2 Model 04-165), shown in Figure 2.5 was employed. The chamber was filled with argon (Ar(g), Linde AG, purity > 99.999%) at room temperature, and subsequently, Ar^+ ions generated by the ion gun were accelerated towards the Pd(111) surface for a duration of 15 min, resulting in surface etching. Following this step, the surface was annealed in UHV for a period of 10 min at 1000 K for surface re-construction/ordering.

Figure 2.5. RBD Model 04-165 2kV backfill ion source (left), and ion source control (right). Adapted from Ref. [64]

2.3.1.2 Cleaning with O_2

The second cleaning procedure involves treating the surface with oxygen to combust C and O-containing species, as Pd is known to be an effective oxidation catalyst. In this method, the Pd(111) surface is directly exposed to O_2 (Linde Ag, purity > 99.999%) through a high

precision leak valve allocated for oxygen dosage for 20 min at 600 K with $P_{O2} = 10^{-8}$ Torr. Subsequently, the surface was subjected to annealing at 1000 K under UHV conditions for a duration of 3-5 min for several times to ensure complete desorption of surface contaminants that are oxidized.

2.3.2 Dosing Ethylene Glycol on Pd(111)

The experimental configuration for introducing ethylene glycol (Aldrich, ≥99%) into the UHV chamber is visually shown in Figure 2.6. Ethylene glycol was contained within a glass finger, which was connected to both a rough pump and a high-precision leak valve via VCR nupro valves, allowing EG passage into the UHV environment. Prior to use, ethylene glycol was purified via multiple freeze-pump-thaw cycles. In this purification technique, the glass bulb, containing EG, was exposed to liquid nitrogen from its outer surface. Once EG was frozen, the VCR nupro valve, connecting the glass bulb and the vacuum, was opened; allowing unfrozen contaminants (i.e., oxygen and nitrogen) to be pumped out. Finally, the purity of the ethylene glycol was confirmed via mass spectrometry. It is important to note that, contaminants with higher freezing point than ethylene glycol, such as water, also froze when the glass bulb was cooled with liquid nitrogen. Thus, such contaminants could not be removed by this technique. A solution to this end, specific to water contamination, is discussed in the next section (2.3.3).

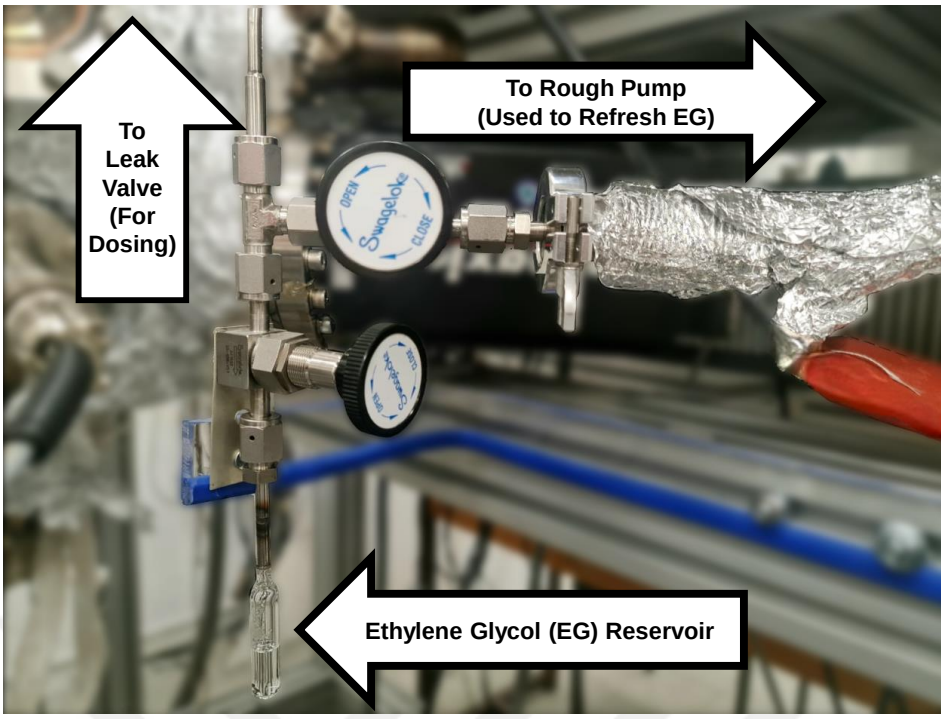

Figure 2.6. Experimental setup for dosing and refreshing (see text) the gas phase ethylene glycol in the gas line via a rough pump.

During the experimentation phase, an important observation was made: the exposed ethylene glycol concentration decreased as the ethylene glycol remained longer within the delivery line. Since the change in ethylene glycol concentration within the delivery line effects the reproducible dosing of ethylene glycol, an experimental procedure was established to obtain reproducible results. Before each ethylene dosing step, the gas-phase ethylene glycol and the existing contaminations in the dosing line was pumped out via rough pump. After the pumping valve was closed, fresh ethylene glycol evaporation was allowed into the dosing line for about 5 min ensuring a controlled ethylene glycol exposure to the UHV chamber with a pressure of 4.5×10^{-11} Torr.

2.3.3 Dosing Temperature of Ethylene Glycol and Oxygen

Ethylene glycol possesses hygroscopic properties, leading to substantial incorporation of water contamination upon air exposure. This effect is demonstrated in Figure 2.7. To

safeguard against water adsorption onto the Pd(111) surface, ethylene glycol was introduced on Pd(111) at a temperature of 200 K in all of the current TPD experiments that is at a temperature where all unwanted H_2O residues already desorb from the Pd(111) surface and do not stick to Pd(111). On the other hand, oxygen was introduced at a lower temperature of 88 K subsequent to the adsorption of ethylene glycol at 200 K. The deliberate cooldown to 88 K and the subsequent oxygen dosing allowed achieving high oxygen coverages on ethylene glycol pre-covered Pd(111) surface as well as monitoring additional oxidation reactions between ethylene glycol and oxygen that may occur at temperatures below 200 K. This strategic ordering of adsorption steps ensured that the catalytic decomposition or oxidation of EG was performed without a significant interference from H_2O contamination.

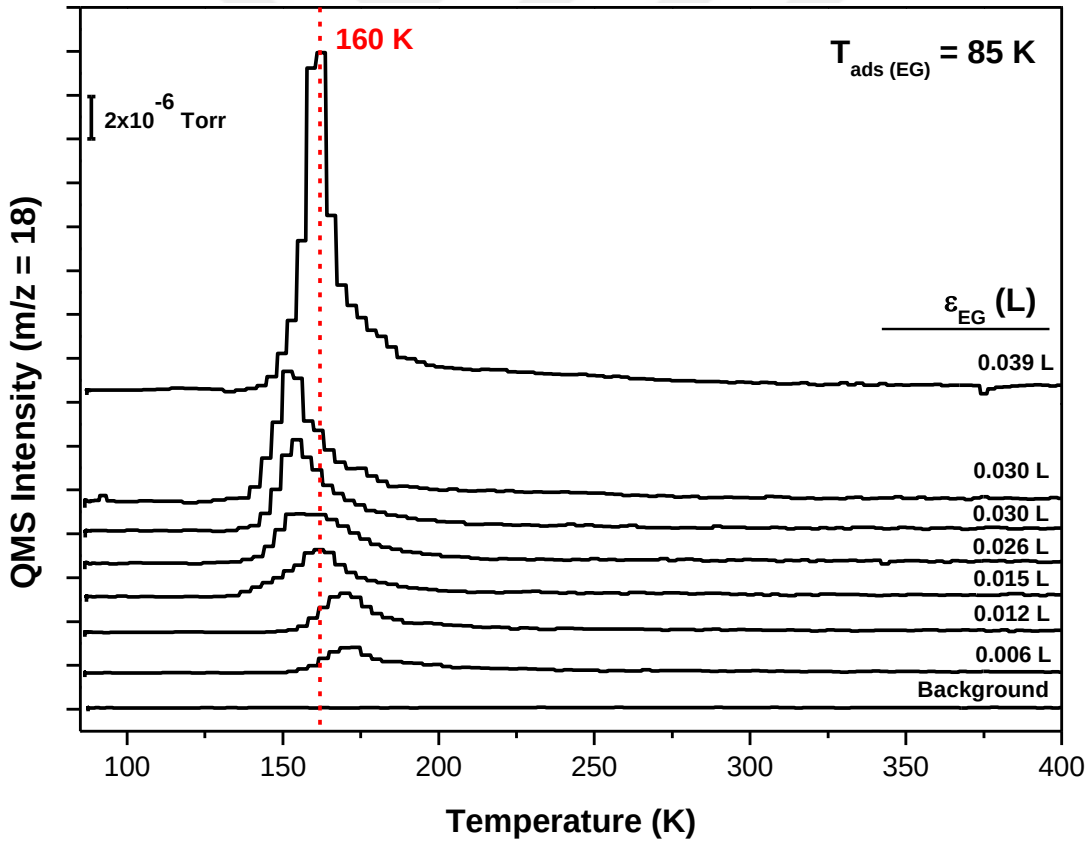

Figure 2.7. m/z = 18 TPD spectra of water evolving as a contamination when increasing exposures of ethylene glycol was dosed on clean Pd(111) at 85 K.

2.3.4 Isotopically Labeled Ethylene Glycol Experiments

In UHV systems, there is always hydrogen molecules as contaminant which can strongly adsorb on Pd(111) surface (T_des > 300 K). To elucidate and understand the effects of background hydrogen on the oxidation reaction, fully isotopically labeled ethylene glycol (OD-CD2-CD2-OD, 98% - Cambridge Isotope Laboratories) was used. As will be discussed in Section 3.2.5, it is found that background hydrogen has no effect on the hydrogenation reaction of surface species.

2.3.5 Choice of Particular Mass Spectroscopic Fragmentation Channels for the Identification of Different Desorption Products in TPD Experiments

In Figure 2.8, fragmentation patterns from the NIST database are displayed for several potential products in EG decomposition and oxidation processes including carbon monoxide, carbon dioxide, ethylene glycol (OH-CH_2-CH_2-OH), glyoxal (-OCHCHO-) , ethylene (C_2H_2), formaldehyde (H_2CO), methanol (CH_3OH), and formic acid (HCOOH).

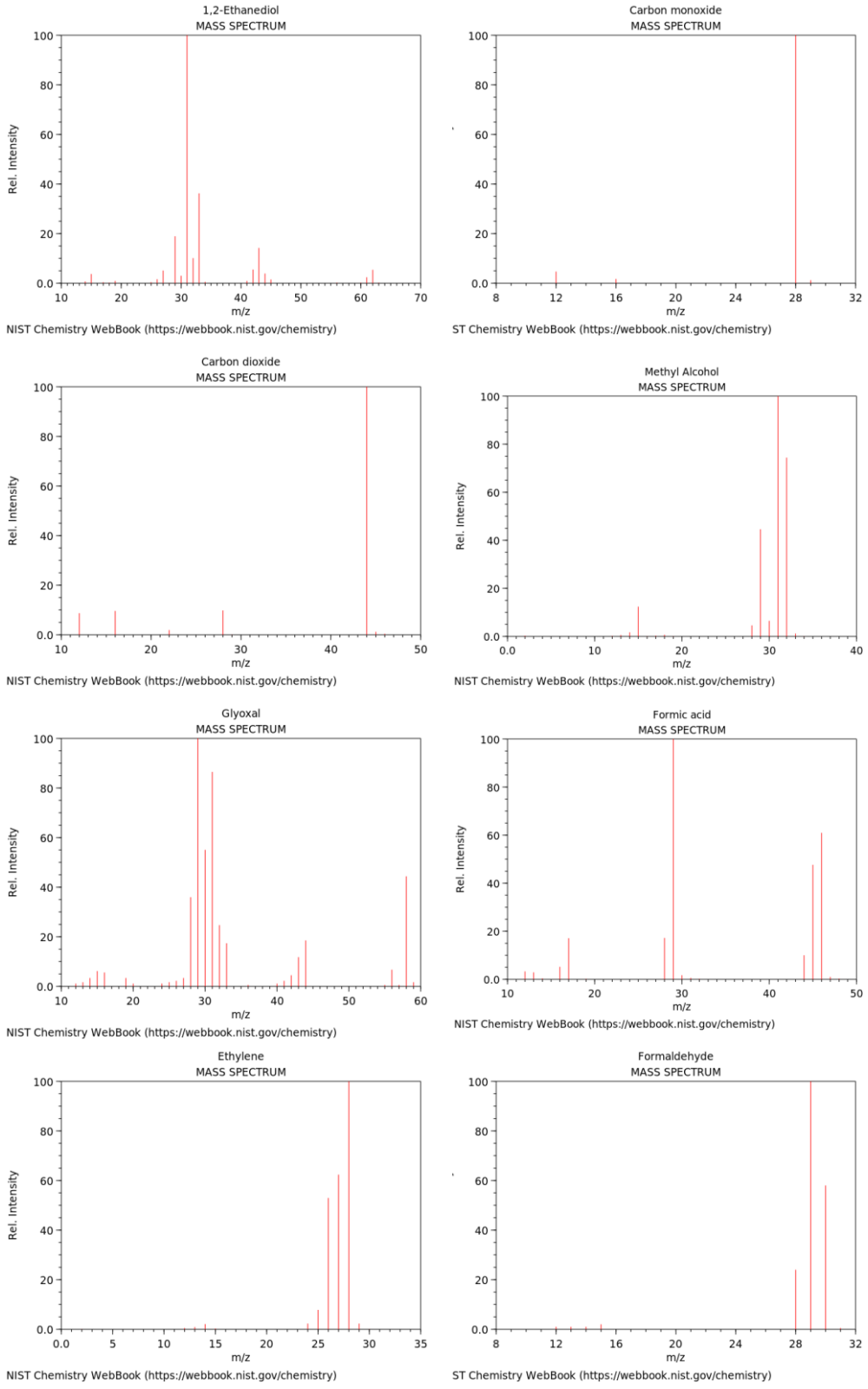

Figure 2.8. Normalized QMS fragmentation patterns of some of the main potential products resulting from the decomposition and oxidation of ethylene glycol on Pd(111). Adapted from Ref. [65]

Both clean and oxidized Pd(111) surfaces were investigated within the range of QMS channels of m/z = 2-67, revealing solely the products presented in Figure 2.9a. Furthermore, Figure 2.9a displays the normalized QMS relative intensities of these products, utilizing the fragmentation patterns from the NIST database as a basis for comparison. Subsequently, Figure 2.9b illustrates the channels selected for each product in our experimental setup. To elucidate, formaldehyde can be detected through both m/z = 29 and m/z = 30. However, if an additional peak appears alongside these channels, with the same shape and temperature, it indicates the presence of glyoxal. It's crucial to acknowledge that the normalized relative intensities of these fragmentations can vary depending on the specific Quadrupole Mass Spectrometer (QMS) used. Consequently, the provided values in Figure 2.9 serve only for estimations of intensities. As an example, Figure 2.10 illustrates how the intensities of various products change when oxygen (PO2 = 1 x 10-8 Torr) is introduced into the UHV system. Notice that m/z = 32, which is oxygen's biggest fragmentation peak, appears as oxygen is introduced into the system. Additionally, peaks of other species slightly increase as well, such as CO (m/z = 28), which comes as contamination with oxygen exposure.

a

Molecules / Channels	2	16	17	18	26	27	28	29	30	31	32	33	44	58	62
Water			20	100											
Glyoxal								100	57	81	25	17	20	45	
Ethylene					57	62	100								
Ethylene Glycol								20		100	10	35			10
Carbon Monoxide							100								
Formaldehyde							25	100	59						
Hydrogen	100														
Oxygen		20									100				
Carbon Dioxide							15						100		

b

Product	Selected Channel
Water	18 (relative intensity = 100)
Hydrogen	2 (relative intensity = 100)
Carbon Dioxide	44 (relative intensity = 100)
Carbon Monoxide	28 (relative intensity = 100)
Ethylene	26 (relative intensity = 57) or (and) 27(relative intensity = 62)
Formaldehyde	29 & 30 (Make sure there is no 58)
Glyoxal	58
1,2 Ethanediol	31
Ethylene Glycol	31
Oxygen	16

Figure 2.9. a) Relative intensities of the QMS fragmentation patterns for each EG decomposition/oxidation product. The channels highlighted in red are the selected channels, and these selections are summarized in the second table presented in b).

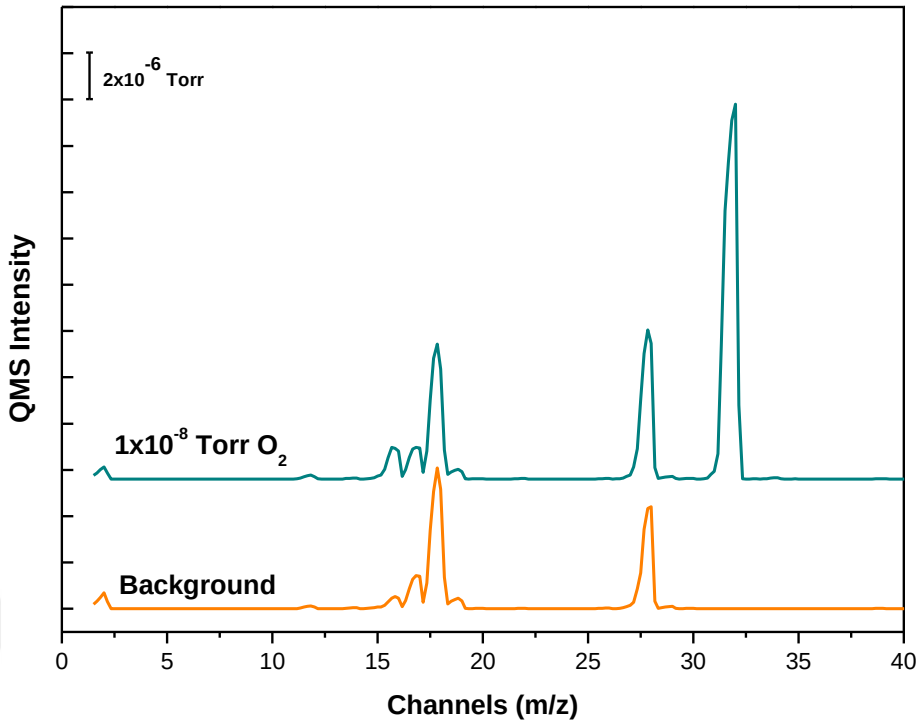

Figure 2.10. The orange curve illustrates the background species detected by the QMS within the UHV system across the mass-to-charge ratio (m/z) range of 2 to 40. Green curve shows the QMS signal when the UHV pressure is intentionally raised to 1 x 10^{-8} Torr through the introduction of oxygen into the system.

Chapter 3

3 - Roles of C_2 Moieties for Ethylene Glycol Oxidation to Formaldehyde and Carbon Dioxide on Pd(111) Single Crystal Model Catalyst Surface

3.1 Ethylene Glycol Adsorption on Pd(111)

Figure 3.1 shows the TPD spectra of varying exposures of ethylene glycol on pristine Pd(111) as monitored by m/z = 31. On this surface, unreacted (i.e., undissociated) ethylene glycol displays two distinct desorption states. One occurs at 220 K and is associated with multilayer ethylene glycol desorption, while the other arises at 260 K and is linked to monolayer ethylene glycol desorption. [49] However, as depicted in Figure 3.1, our findings provide evidence indicating the concurrent development of both states, even when the coverage of ethylene glycol was extremely low.

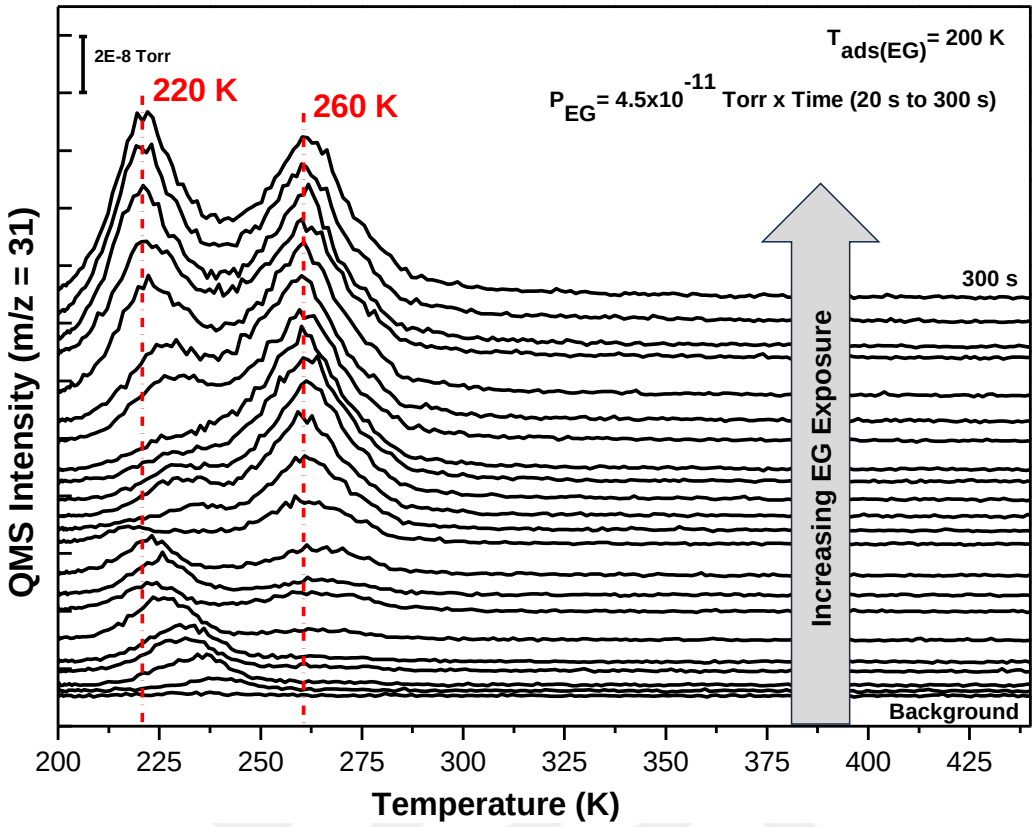

Figure 3.1. TPD spectra for various exposures of ethylene glycol on clean Pd(111) surface at 200 K. Exposure time in s (bottom to top); 0 (background), 20, 25, 30, 35, 40, 45, 50, 55, 60, 65, 70, 75, 80, 85, 90, 95, 100, 105, 180, 240, 300.

This observation implies that intermolecular interactions among ethylene glycol molecules prompt a growth pattern resembling clusters, rather than the formation of multiple layers after the initial monolayer is formed. A similar phenomenon has also been documented on the Ag(110) surface.[51] Figure 3.2 depicts the primary modes of adsorbate growth on a substrate. According to these growth modes, the adsorption of ethylene glycol on Pd(111) (as shown in Figure 3.1) resembles the Volmer-Weber (island) growth mode at low coverages. As the coverage increases, the growth mode transitions into a combination of both Volmer-Weber (island) and Stranski-Krastanov (layer + island) growth modes.

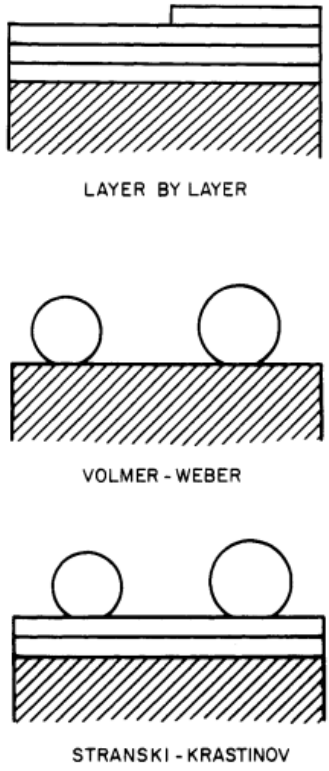

Figure 3.2. a) Frank-van der Merve (layer-by-layer) growth mode; b) Volmer-Weber (island/cluster) growth mode, c) Stranski-Krastanov (layer +island) growth mode. Adapted from Ref. [66]

3.2 Behavior of Ethylene Glycol in the Presence of Oxygen on Pd(111)

3.2.1 Effects of Oxygen on Molecular Desorption of Ethylene Glycol

Upon the introduction of oxygen to the Pd(111) surface which was initially exposed with ethylene glycol, the molecular desorption states of ethylene glycol, previously observed at 200 K and 220 K vanish as illustrated in Figure 3.3. This change suggests that the presence of oxygen results in the complete catalytic consumption of ethylene glycol. This phenomenon can be attributed to the stabilizing influence of atomic oxygen, which compels unreacted ethylene glycol to remain on the surface, eventually undergoing oxidation or decomposition. A similar behavior was also reported for ethanol adsorption Rh(111) and Rh(100) surfaces, in which it desorbs without reacting with the surface. However, ethanol dissociates on oxidized Rh(111)

and Rh(100).[67] Subsequent to a specific exposure to ethylene glycol, the Pd(111) surface becomes poisoned by it (not shown), particularly due to its dosing prior to oxygen introduction. This ultimately leads to observing the same behavior in the case of a pristine Pd(111) surface (i.e. only decomposition of ethylene glycol).

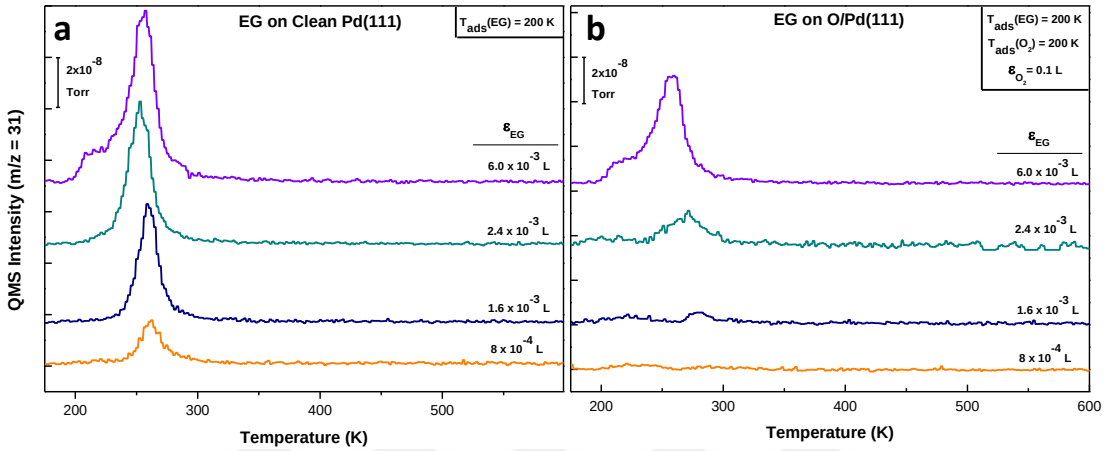

Figure 3.3. Molecular desorption of ethylene glycol (m/z = 31) on a) clean and b) oxygen exposed Pd(111) surfaces. Oxygen was dosed at 1 x 10^{-9} Torr for 1 min at 88 K after the exposure of ethylene glycol.

3.2.2 Effects of Oxygen on Water and Hydrogen Formation from Ethylene Glycol

Figure 3.4 shows the TPD profiles of hydrogen desorption upon adsorption of ethylene glycol on both pristine (orange) and oxidized (blue) Pd(111) surfaces at 200 K. Formation of ethylenedioxy (-OCH_2CH_2O-) from ethylene glycol occurs above 140 K, releasing hydrogen onto the surface.[49] This phenomenon also readily occurs in our experiments, since ethylene glycol was introduced at 200 K (Figure 3.3). In the absence of oxygen on the surface, adsorbed hydrogen atoms generated due to ethylene glycol dehydrogenation desorb in a recombinative fashion to form H_2, as shown in equation 3.1 and 3.2.

$$H(a) + H(a) \rightarrow H_2(a) \tag{3.1}$$

$$H_2(a) \rightarrow H_2(g), \qquad at\ 330\ K \tag{3.2}$$

However, in the presence of oxygen on the surface, the hydrogen desorption diminishes as compared to that of the clean Pd(111) surface (e.g., compare H_2-TPD data for 0.0009 L EG adsorbed on clean and oxygen pre-dosed Pd(111) surfaces in Figure 3.4b). On the other hand, further increase in the ethylene glycol exposure results in a corresponding increase in hydrogen desorption yield, attributed to enhanced dehydrogenation processes.

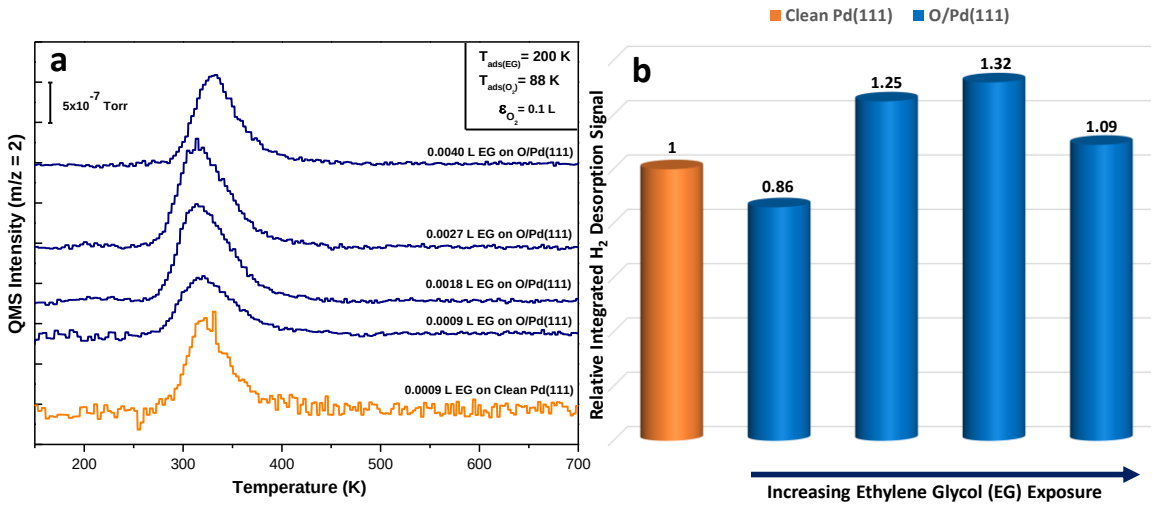

Figure 3.4. a) TPD profiles of hydrogen desorption (m/z = 2) with various exposures of ethylene glycol at 200 K on both clean (orange) and oxidized (blue) Pd(111) surfaces. b) Relative integrated desorption signals of hydrogen. Oxygen was dosed at 1 x 10^{-9} Torr for 1 min at 88 K after the exposure of ethylene glycol.

The reduction in hydrogen desorption, in comparison to the pristine Pd(111) surface for low ethylene glycol coverages, can be attributed to the formation of water, a phenomenon exclusively observed on the oxidized Pd(111) surface.[26], [68], [69] In Figure 3.5, TPD spectrum of water both on clean and oxidised Pd(111) surfaces provided, showing two distinct

states of water desorption at 190 K and at 250 K. As discussed before, previous investigations into the formation of water from carboxylic acid dehydrogenation on Pd(111) have provided insights indicating the occurrence of both OH disproportionation and O + H reactions along with OH + H reaction on this surface. [26], [68], [69] The OH disproportionation process transpires between 190 K and 200 K, while the O + H reaction takes place above 240 K.

$$RCH_2OH(a) + O(a) \rightarrow RCH_2O(a) + OH(a) \quad (1.1)$$

$$RCH_2OH(a) + OH(a) \rightarrow RCH_2O(a) + H_2O(a), \quad (below\ 190\ K) \quad (1.2)$$

$$H_2O(a) \rightarrow H_2O(g), \quad (above\ 190\ K) \quad (1.3)$$

$$OH(a) + OH(a) \rightarrow H_2O(g), \quad (above\ 190\ K) \quad (1.4)$$

$$2H(a) + O(a) \rightarrow H_2O(g), \quad (above\ 240\ K) \quad (1.5)$$

Consequently, in Figure 3.4, we associate the water desorption peak at 190 K with both the OH disproportionation and OH + H reaction, which has also been noted in alcohol oxidation reactions. [25] The presence of a second peak, coinciding with the tail of the first peak, occurs around 250 K and is attributed to the O + H reaction.

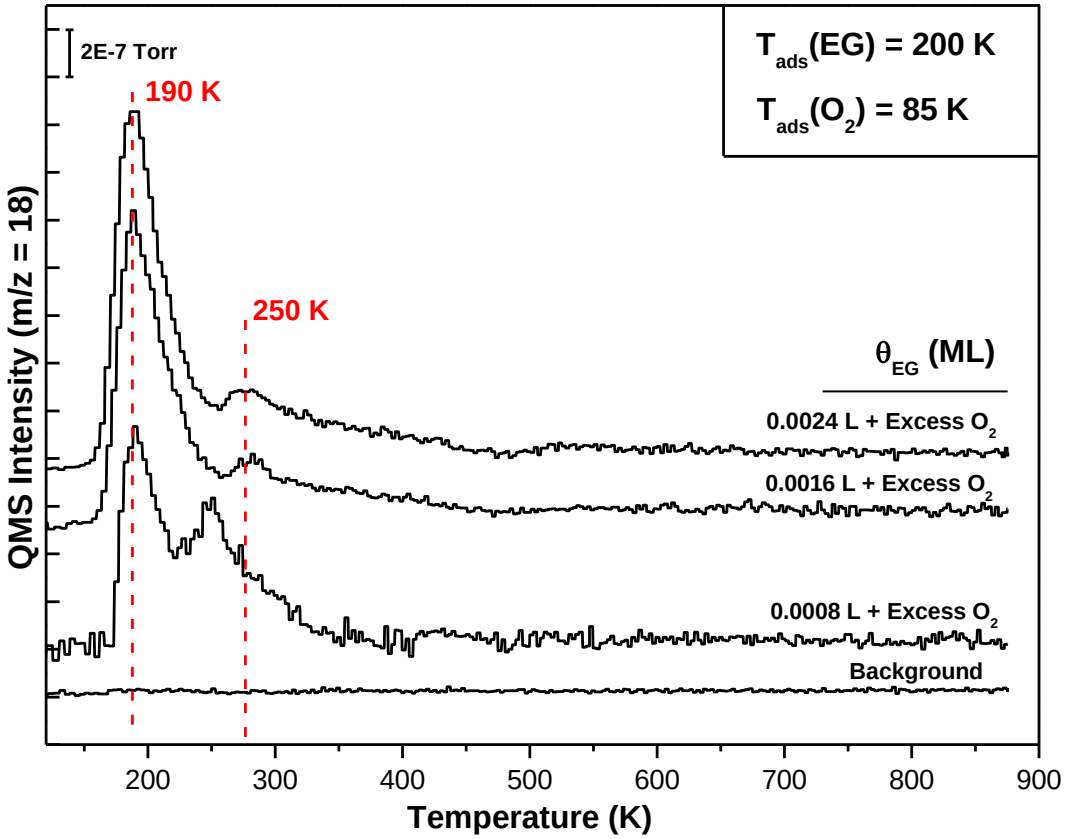

Figure 3.5. TPD spectra of water (m/z = 18) for various exposures of ethylene glycol at 200 K and fixed exposure of oxygen (P_{O2} = 1 x 10^{-9} Torr, 1 min, at 85 K) on Pd(111).

3.2.3 Effects of Oxygen on CO Formation from Ethylene Glycol

Figure 3.6 displays the TPD profile of CO on both clean and oxidised Pd(111) upon exposure of ethylene glycol at 200 K. On clean Pd(111), CO was already reported as the dominant product.[49] Notably, the presence of surface oxygen atoms amplifies its formation, as depicted in Figure 3.6a. Beyond a specific ethylene glycol exposure threshold, specifically at 0.0040 L, the surface becomes susceptible to ethylene glycol-induced poisoning, resulting in a reduction in the intensity of carbon monoxide desorption. Moreover, the presence of surface oxygen species facilitates the generation of carbon dioxide, which will be discussed in the next section in detail. Note that desorption peaks of CO_2 below 400 K were not observed on pristine

Pd(111) [49], when ethylene glycol is exposed to the clean Pd(111) surface. Further elaboration on the origins of these CO_2 and CO peaks will be provided in the subsequent section.

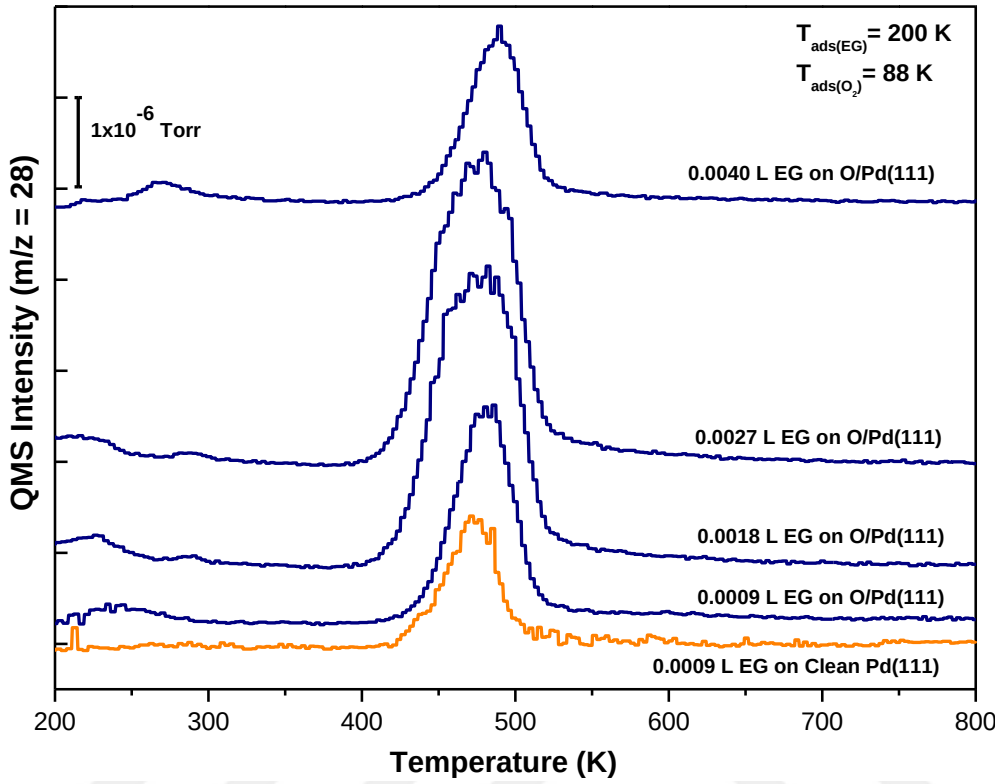

Figure 3.6. TPD profile of CO (m/z = 28) when ethylene glycol dosed on clean (orange curve) and oxidized Pd(111) at 200 K. Oxygen (P_{O2} = 1 x 10^{-9} Torr, 1 min, at 85 K) dosed after the adsorption of ethylene glycol.

3.2.4 Some of the Possible C_2 Surface Moieties Yielding CO_2 and H_2CO

Figure 3.7 shows the desorption profiles of CO_2 and formaldehyde (H_2CO) when various exposures of ethylene glycol reacted with oxygen on Pd(111). The evolution of formaldehyde results from the C-C bond cleavage of -OCH_2CH_nO- surface intermediates, where *($n \leq 2$)*.[51] Similar to simple alcohol reactions on Pd(111)[23], [26], oxygen acts as a strong nucleophile, facilitating the scission of the C-C bond and ultimately leading to the formation of two different surface moieties: H_2CO and OCH_nO. In this context, our focus

narrows to cases where atomic oxygen attacks the second carbon (-CH_nO-) of the -OCH_2CH_nO- species. This choice enables us to elucidate the origins of potential surface species and rationalize the temperatures at which the observed products undergo desorption.

In Figure 3.7a, formaldehyde desorption occurs at three different temperatures namely; 200 K, 220 K, and 280 K. Starting with the highest temperature; 280 K peak is attributed to paraformaldehyde (-CH_2O-)$_n$ decomposition. As discussed in section 1.3.3, investigations into aldehyde adsorption at 170 K, both on pristine and oxidized Pd(111), have demonstrated that formaldehyde undergoes polymerization, resulting in the formation of paraformaldehyde.[37] Decomposition of paraformaldehyde occurred at 260 K and 280 K, respectively on Pd(111) and Rh(111) surfaces, supporting the argument that the 280 K peak of formaldehyde desorption in Figure 3.7a originates from the paraformaldehyde decomposition.[37]–[39] However, this 280 K peak of formaldehyde in Figure 3.7a, is not observed at low EG/O ratios. Studies have underscored the pivotal role of formyl species as initiators in this polymerization process on Pd(111), Rh(111) and Ag(110). [38], [39], [41] Additionally, formaldehyde adsorption on Rh(111)-(2x2)O surface has shown that the average chain length of the paraformaldehydes decreases from 9.4 to 5.9 when the CO coverage is increased on the surface.[38] Thus, the absence of the 280 K peak of formaldehyde at lower ethylene glycol coverages shown in Figure 3.7a either suggests the absence of formyl species on the surface or their inhibition due to other products like CO. However, as previously shown in Figure 3.6a, CO intensity increases with increasing coverage of ethylene glycol. Therefore, the lack of paraformaldehyde decomposition at 280 K for low ethylene glycol coverages cannot be attributed to CO inhibition, as CO coverage is higher when paraformaldehyde decomposition is observed. Another study, investigating ethanol oxidation on Rh(111) and Rh(100) suggested that the enhanced CH_4 formation on oxidised surface is due to the presence of surface oxygen atoms, which inhibits the hydrogen binding sites, preventing the dehydrogenation of surface hydrocarbons.[67] It is

possible that at high coverage exposure of ethylene glycol (i.e., Figure 3.7a – green curve) lack of oxygen on the surface leads to formyl formation as a result of formaldehyde dehydrogenation so that polymerization can occur. Additionally, while the desorption intensity of formaldehyde at 280 K in Figure 3.7a remains relatively modest, it is essential to acknowledge that carbon monoxide emerges as the predominant product of paraformaldehyde decomposition. The increased carbon monoxide desorption discussed in section 3.2.3 (see Figure 3.6a), compared to the reaction of ethylene glycol on pristine Pd(111), further supports this assertion.

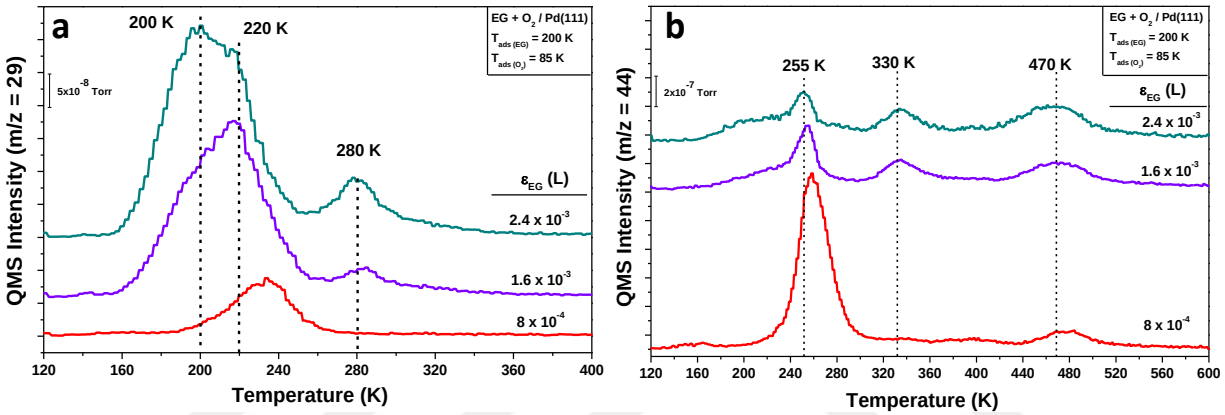

Figure 3.7. TPD spectra of a) formaldehyde (H_2CO, m/z = 29), b) CO_2 (m/z = 44) upon the exposure of ethylene glycol at 200 K on O/Pd(111). Oxygen (P_{O2} = 1 x 10^{-9} Torr, 1 min, at 88 K) dosed after the adsorption of ethylene glycol.

Figure 3.7a also shows two formaldehyde peaks at 200 K and 220 K, which have not been reported so far on either pristine or oxidised Pd(111).[37], [39] Formaldehyde also exhibits weak binding on Rh(111) surface and desorbs below 150 K.[38] Consequently, the formaldehyde peaks at 200 K and 220 K in Figure 3.7a are ascribed to reaction-limited products originating from the bond scission of C_2 surface species ($-OCH_2CH_nO-$) and desorb instantaneously. The 20 K temperature difference between these two states of formaldehyde desorption is assumed to be related with the relative stability of originating C_2 surface species. Previous theoretical calculations have also shown that as dehydrogenation occurs, the stability

of the C_2 intermediate decreases, making C-C bond scission favorable.[34], [52] Based on these studies, in our case, the stability of C_2 surface species (-OCH_2CH_nO-) decreases as *n* decreases. As a result, 200 K desorption of formaldehyde is attributed C-C bond scission of -OCH_2CO- *(n = 0)* surface species, which is assumed to be the least stable C_2 surface species in terms of C-C bond stability.

Furthermore, origins of the 200 K and 220 K formaldehyde desorption signals can be further supported by analyzing the CO_2 formation. Figure 3.7b shows the desorption profiles of CO_2 when various exposures of ethylene glycol reacted with oxygen on Pd(111). In case of -OCH_2CO- *(n = 0)* surface specie, nucleophilic attack of atomic oxygen on the second carbon leads to CO_2 formation as well as formaldehyde. Temperature of C-C bond scission can be roughly monitored by the evolution of CO_2, as it is known to weakly bind to Pd(111), desorbing at approximately 100 K.[59]. The simultaneous evolution of CO_2 (Figure 3.7b) and H_2CO (Figure 3.7a) at 160 K suggest the presence of the readily occurring -OCH_2CO- surface species, wherein oxygen attacks the second carbon and leads to C-C bond scission at this temperature yielding H_2CO and CO_2 simultaneously. It is worth noting that the higher desorption intensity of H_2CO compared to CO_2 at 160 K indicates the presence and C-C bond activation of other C_2 surface species with $n > 1$. Hence, although the 200 K peak of formaldehyde in Figure 3.7a is mainly attributed to the -OCH_2CO- (*n = 0)*, the contribution from other C_2 species with $n > 1$ (such as -OCH_2CHO- and -OCH_2CH_2O-) cannot be excluded. A brief illustration for the C-C bond scission of the -OCH_2CO- *(n = 0)* surface specie as a result of atomic oxygen's attack is provided in Figure 3.8a. [43], [69][59] On the other hand, 220 K desorption of formaldehyde in Figure 3.7a can be attributed to both -OCH_2CHO- *(n = 1)* and -OCH_2CH_2O- *(n = 2)*. Starting from the former, the nucleophilic attack of atomic oxygen to the second carbon of -OCH_2CHO- (*n = 1)*, leads to formation of formaldehyde (H_2CO) and surface formate (-$OCHO^-$). Formaldehyde desorbs from the surface as soon as it is formed which we attribute to 220 K

desorption. Formate, on the other hand, undergoes decomposition to yield surface hydrogen and CO_2, a reaction occurring above the threshold of 260 K.[26], [68] Consequently, it can be inferred that the initial peak of CO_2 observed at 260 K in Figure 3.7b is likely a consequence of the decomposition of formate. This specific peak experiences a shift to 255 K in response to an escalation in the EG/O ratio, potentially attributable to surface overcrowding dynamics. An illustration for the C-C bond scission of the -OCH_2CHO- *(n = 1)* surface specie as a result of atomic oxygen's attack provided in Figure 3.8b.

Finally, the last possible species that can produce formaldehyde is -OCH_2CH_2O- *(n = 2)*. Nucleophilic attack of atomic oxygen upon the -OCH_2CH_2O- *(n = 2)*, leads to the creation of dioxymethylene (-OCH_2O-) and formaldehyde.[51] As stated in previous paragraph, 220 K peak of formaldehyde in Figure 3.7a may also originate from -OCH_2CH_2O- *(n = 2)* along with -OCH_2CHO- *(n = 1)*. On the other hand, dioxymethylene is an unstable intermediate and manifests two competing reaction pathways: one involving the generation of paraformaldehyde $(H_2CO)_n$ and the other involving dehydrogenation leading to surface-bound formate ($HCOO^-$).[29], [31], [37], [40], [51] Paraformaldehyde, upon decomposition, contributes to the formation of formaldehyde, carbon monoxide, and surface hydrogen. [29], [37]–[39] Unfortunately, the distinction between the formation of formaldehyde from paraformaldehyde and methoxy decomposition remains elusive. Moreover, it is important to note that -OCH_2CH_2O- *(n = 2)* surface specie acts as an inherently unstable intermediate and is prone to dehydrogenation, transforming into glyoxal (-OCHCHO-) beyond 170 K on an pristine Pd(111) surface.[49] Consequently, its potential influence on the overall reaction is considered to be minimal in comparison to the (-OCH_2CH_nO-) intermediates, where *n* varies. An illustration for the C-C bond scission of the -OCH_2CH_2O- *(n = 2)* surface specie as a result of atomic oxygen's attack provided in Figure 3.8c.

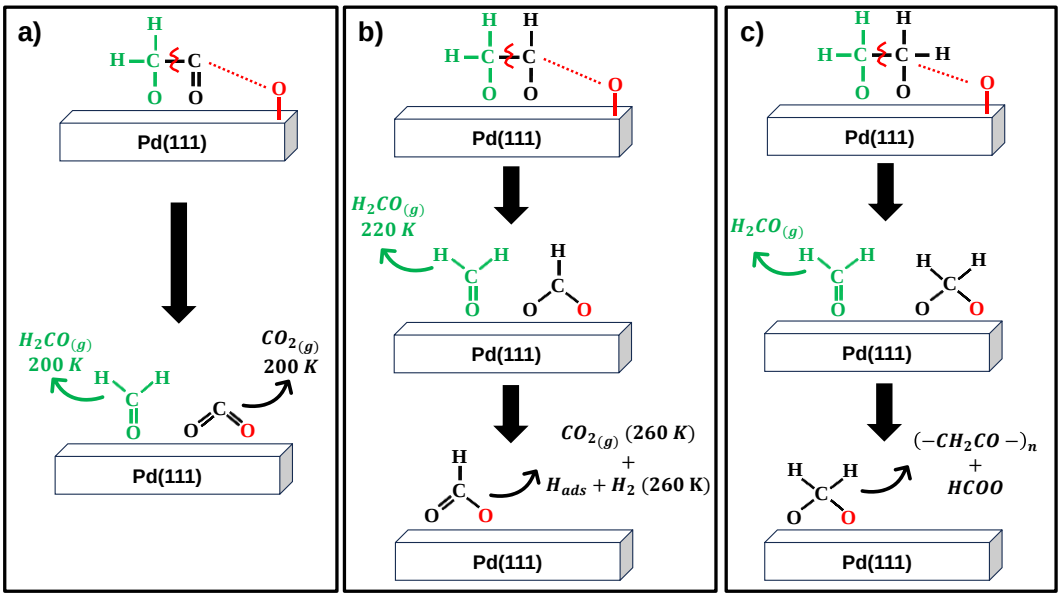

Figure 3.8. Illustration of likely surface intermediates a) -OCH_2CO-, b) -OCH_2CHO-, c) -OCH_2CH_2O- interacting with atomic oxygen on the Pd(111) surface and yielding formaldehyde as a product.

By exploring various EG/O coverages, dependence of oxidation product selectivity on relative amounts of reactants can be explained. Figure 3.9 shows the normalized relative amounts of formation of CO_2 and formaldehyde on oxidised Pd(111) with the varying EG/O ratios (i.e., integrated peak areas obtained from the TPD desorption signals in Figure 3.7) Note that ethylene glycol was dosed first onto the surface at 200 K, followed by oxygen at 85 K. Thus, as ethylene glycol coverage increased, oxygen coverage decreased. At low EG/O coverages, indicative of an oxygen surplus, CO_2 prevails as the main oxidation product. As the EG/O ratio is increased, formaldehyde and CO_2 formation becomes equal (moderate oxygen in Figure 3.9) and finally formaldehyde formation exceeds the CO_2 (low oxygen in Figure 3.9). As the EG/O ratio is even further increased, signifying an excess of ethylene glycol, a reduction in the intensity of the 260 K desorption peak associated with CO_2, stemming from formate decomposition, is observed (in Figure 3.7b). Concurrently, a peak at 335 K arises in Figure 3.7b, attributed to glyoxal oxidation, and exhibits a slight augmentation in intensity. These

observations suggest that in scenarios where there is an abundance of oxygen on the surface, its influence extends beyond merely facilitating the cleavage of the C-C bond within the (-OCH_2CH_nO-) intermediate by interacting with the (CH_nO-) group. Accordingly, additional oxygen atoms also engage with the (-OCH_2) moiety of the molecule, resulting in a deterrent effect on the formation of formaldehyde. Importantly, the excess oxygen further limits the production of paraformaldehyde, evident in the absence of a 280 K peak in Figure 3.7a corresponding to formaldehyde in cases of low EG/O ratios. This effect of oxygen concentration underscores the pivotal role of one-sided oxygen attack upon C_2 surface species in the context of formaldehyde formation.

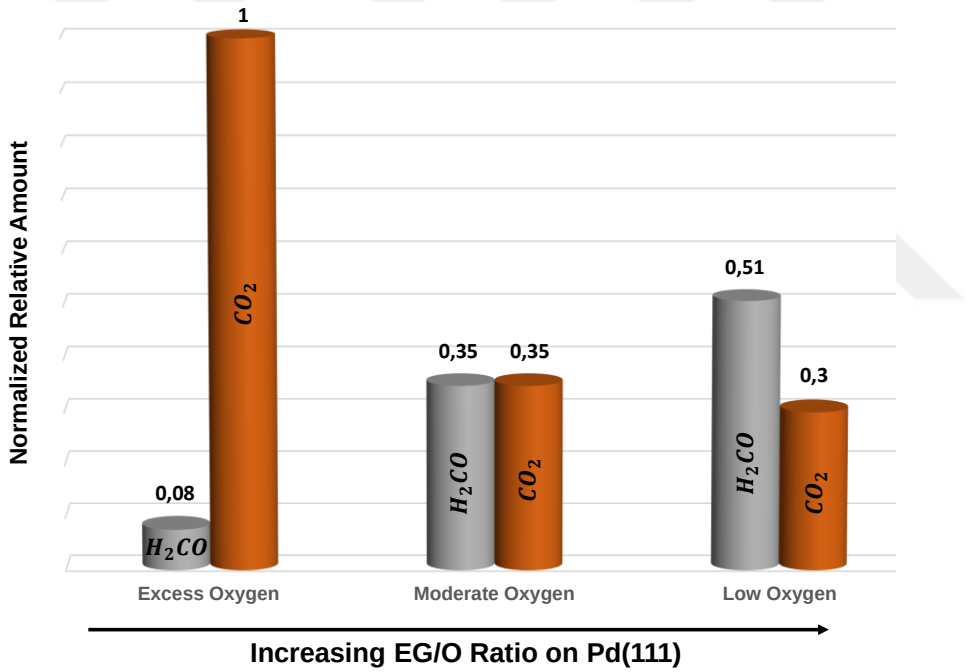

Figure 3.9. Normalized relative yields of formaldehyde (grey) and CO_2 (orange) shown as a function of increasing EG/O ratio from left to right. EG/O ratios include the following ratios of EG/O: "Excess Oxygen" = 8 x 10^{-3} (8 x 10^{-4} L / 0.1 L), "Moderate Oxygen" = 1.6 x 10^{-2} (1.6 x 10^{-3} L / 0.1 L), "Low Oxygen" = 2.4 x 10^{-3} (2.4 x 10^{-4} L / 0.1 L). Note that actual surface *coverage* of adsorbed oxygen depends on the exposed ethylene glycol since oxygen dosed after ethylene glycol.

3.2.5 Isotopically Labeled Ethylene Glycol ($DOCD_2CD_2OD$) Experiments on O/Pd(111) Surface

Figure 3.10 shows the m/z = 29, 30, 31, and 32 TPD desorption channels measured upon adsorption of fully deuterated ethylene glycol ($DOCD_2CD_2OD$) followed by oxygen on Pd(111). Among these 4 desorption channels, only two of them revealed significant desorption intensities, namely; m/z = 30 (H_2CO or fragmentation of D_2CO) and m/z = 32 (D_2CO). This outcome signifies the absence of HDCO (m/z = 31) formation. Furthermore, if m/z = 30 were due to H_2CO, the presence of m/z = 29 would be also anticipated due to fragmentation, yet this is not observed. Accordingly, m/z = 32 corresponds to D_2CO, while the observed m/z = 30 represents its fragmentation pattern. This observation implies that subsequent to the creation of a formyl group, its hydrogenation reaction remains elusive, matching with prior investigations on formaldehyde which solely reported formaldehyde decomposition but not its hydrogenation.[37], [39] Consequently, it is highly probable that other C_2 surface species, such as -OCHCHO- and -OCHCO-, do not yield formaldehyde via C-C bond scission and formyl (-OCH) hydrogenation. Crucially, this underscores that the hydrogenation of formyl does not occur on the Pd(111) surface. Therefore, reaction routes aimed at formaldehyde production should originate from more intricate structures and precisely halt at the stage of formaldehyde formation. It is noteworthy that the desorption of m/z = 32 at temperatures below 200 K in Figure 3.10 stems from the desorption of molecular oxygen species. From the experiments of non-deuteriated version of ethylene glycol, we did not observe any m/z = 32 signal which proves the fact that this signal comes from the D_2CO and not O_2 . Additionally, the peak observed at 475 K for m/z = 29 originates from ethylene desorption and is unrelated to formaldehyde.

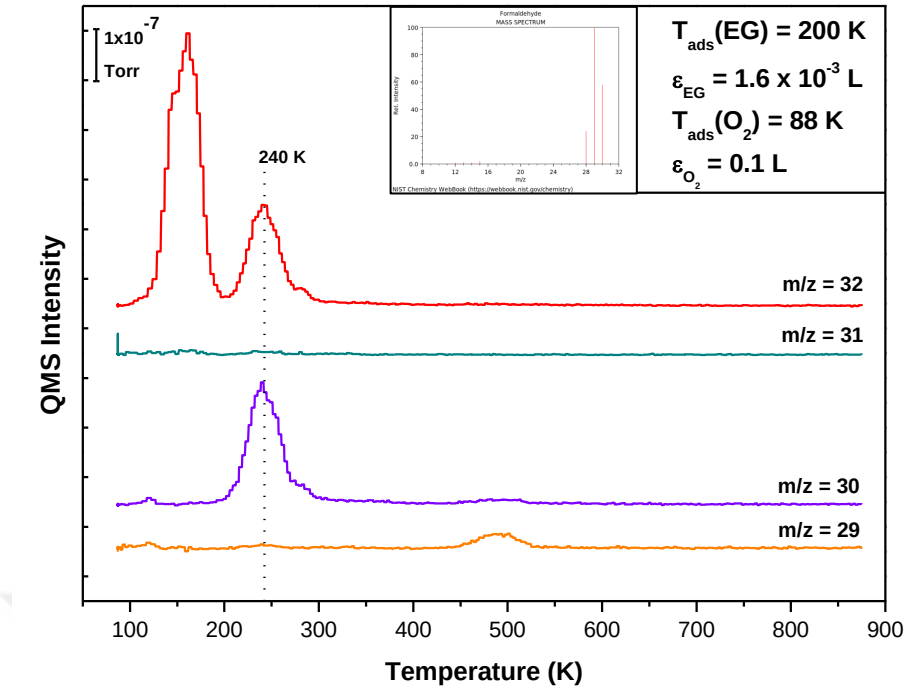

Figure 3.10. TPD channels corresponding to H_2CO (M_W = 30 g/mol), D_2CO (M_W = 32 g/mol), and HDCO (M_W = 31 g/mol) desorption. The inset figure is adapted from Ref. [65]

3.2.6 Roles of Other C_2 Surface Moieties

Based on our isotopically labeled ethylene glycol experiments, it is highly likely that other C_2 surface intermediates, such as -OCHCHO- and -OCHCO- do not yield any formaldehyde through C-C bond scission and formyl (-OCH) hydrogenation. Based on these findings, the 340 K peak of CO_2 in Figure 3.7b can be attributed to the C-C bond scission of -OCH_nCH_nO- *(n ≤ 1)* surface species. Specifically, this desorption peak may be originating from unreacted glyoxal (-OCHCHO-, *n = 1*) which is reported to be stable up to 470 K on clean Pd(111).[49] The remaining glyoxal may either form CO as a result of C-C bond scission or surface ethyne through C-O bond cleavage. Surface ethyne either decomposes to surface hydrogen and carbon or desorb as ethylene by abstracting hydrogen from the surface.[49], [50] An illustration of C-C bond cleavage of glyoxal (-OCHCHO-) as a result of its interaction with

atomic oxygen and the resulting surface species along with the products provided in Figure 3.11a.

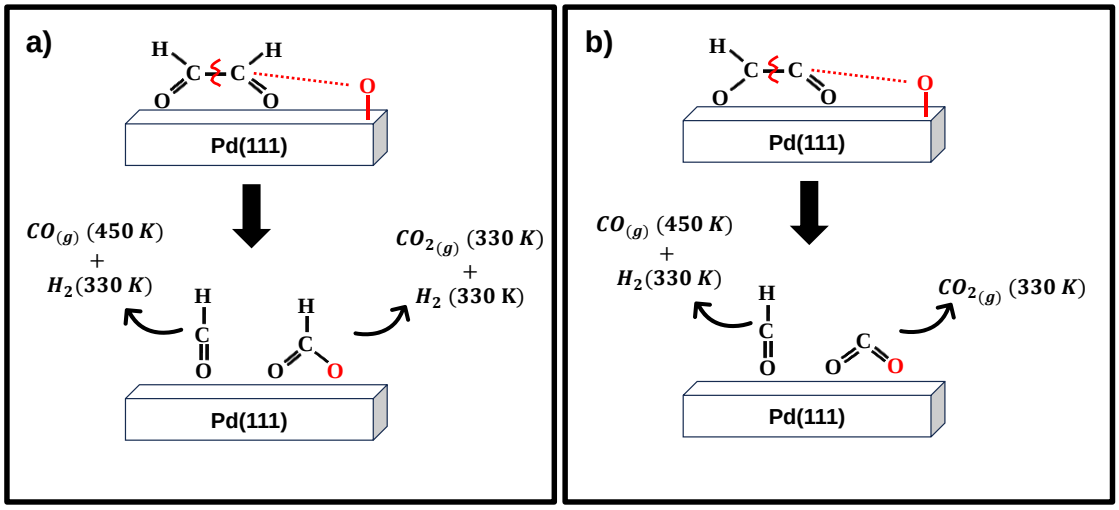

Figure 3.11. Reaction pathways of atomic oxygen with the C_2 intermediates a) -OCHCHO-, b) -OCHCO- yielding CO, H_2, and CO_2, without producing formaldehyde.

Lastly, the 465 K peak of CO_2, in Figure 3.7b, is attributed to CO + O reaction. We also observed this peak, albeit with a smaller intensity when ethylene glycol was exposed on pristine Pd(111) (not shown). In the case of clean Pd(111), it is likely that atomic oxygen formed through C-O bond scission of glyoxal reacts with the surface CO and forms CO_2. Increase in the desorption intensity of CO_2 at 465 with increasing EG/O ratio (Figure 3.7b) further supports this claim. Finally, notice that after the initial desorption of CO_2, the baseline in desorption channel m/z = 44 (CO_2) in Figure 3.7b does not return to initial level, indicating the continuous formation and desorption of the -OCH_nCH_nO- ($n \leq 2$) species. This dynamic behavior underscores the complex nature of ethylene glycol oxidation.

3.2.7 Ethylene Glycol on Pd(111) vs O/Pd(111)

Overall, our results indicate that the oxygenated Pd(111) surface exhibits a higher efficiency in the conversion of ethylene glycol compared to pristine Pd(111), as evidenced by

the desorption of a greater variety of carbon-containing products (Figure 3.6). The presence of surface oxygen promotes the formation of diverse surface intermediates, including formate and likely dioxymethylene (Figure 3.8 and Figure 3.11). This enhanced reactivity is consistent with previous observations on alcohol conversion on Rh(111) and Pd(111).[69], [70]

Comparing the oxidation of ethylene glycol with ethanol on oxidized Pd(111), both reactions involve the initial breaking of the O-H bond, leading to alkoxide intermediates. For ethanol, subsequent C-C bond cleavage results in acetaldehyde desorption, peaking at 170 K.[69] Note that acetaldehyde was not observed when ethanol decomposed on pristine Pd(111).[23] On the other hand, for ethylene glycol, first and second C-H bond activations of the (-OCH_2CH_nO-) moiety from (CH_nO-) side followed by C-C bond scission led to two different formaldehyde desorption states at 220 K and 200 K, respectively (Figure 3.7a) . The C-C bond scission of ethanol on Pd(111) is only observed through the desorption of CH_4 at 330 K, indicating ethylene glycol is much more prone to C-C bond cleavage. [22], [25] Additionally, ethanol oxidation also led to formation of acetic acid and CO_2. [25], [31], [38]Although we did not observe desorption of any carboxylic acidic products such as formic acid, glycolic acid, etc., their non-existence on the surface must be further verified by further vibrational spectroscopic studies.

Finally, the oxidation of ethylene glycol on Pd(111) exhibits quite similar products with the oxidation of 1,2-ethanedioxy on Ag(110).[51] However, while the oxidation 1,2-ethanedioxy on Ag(110) results in ethylene glycol desorption at 230 K, 250 K, and 395 K, atomic oxygen on Pd(111) reacts and consumes the molecularly adsorbed ethylene glycol which is observed on pristine Pd(111) (Figure 3.3). In this sense, Pd(111) may exhibit a better catalytic conversion of polyols compared to Ag(110) surface.

Chapter 4

Conclusion

Upon introducing ethylene glycol at 200 K onto the Pd(111) surface, a variety of surface species -OCH_nCH_nO-, where $n \leq 2$, are formed. The interaction between atomic oxygen and -OCH_2CO- initiates the concurrent desorption of CO_2 and formaldehyde, with formaldehyde exhibiting a distinct peak at 200 K. A slightly more stable specie -OCH_2CHO-, in terms exhibiting a stronger C-C bond stability, leads to formaldehyde desorption at 220 K and subsequent CO_2 release at 255 K, driven by formate decomposition. Additionally, the emergence of paraformaldehyde, originating from both dioxymethylene and formaldehyde, undergoes a decomposition process, yielding a final formaldehyde peak at 280 K. Meanwhile, surface species such as OCHCHO- and -OCHCO- are deemed plausible contributors to CO_2 desorption at 330 K, while CO oxidation becomes the predominant factor for desorption at 460 K.

The early temperature desorption of formaldehyde, starting at 150 K, shows the necessity of C-C bond scission, facilitated in the presence of oxygen, before the C-H bond activation of C_2 surface species. On the other hand, when there is excess atomic oxygen, more than one oxygen atom interacts with both of the carbons of a C_2 intermediate, enhancing the total oxidation product: CO_2. It is presumed that exposing ethylene glycol at 200 K may reduce the yield of formaldehyde since C-H bond activation already initiates at 170 K. While emphasizing the importance of exposing ethylene glycol at 200 K to prevent water accumulation on the surface, further studies should elucidate the effects of water on polyol reactions. These investigations will not only aid in the design of improved catalysts for formaldehyde formation at temperatures below 200 K but also shed light on the inevitable influence of water on polyol reactions.

Bibliography

[1] F. W. Lichtenthaler and S. Peters, “Carbohydrates as green raw materials for the chemical industry,” *Comptes Rendus Chimie*, vol. 7, no. 2, pp. 65–90, Feb. 2004, doi: 10.1016/j.crci.2004.02.002.

[2] A. Corma, S. Iborra, and A. Velty, “Chemical Routes for the Transformation of Biomass into Chemicals,” *Chem Rev*, vol. 107, no. 6, pp. 2411–2502, Jun. 2007, doi: 10.1021/cr050989d.

[3] G. W. Huber, S. Iborra, and A. Corma, “Synthesis of Transportation Fuels from Biomass: Chemistry, Catalysts, and Engineering,” *Chem Rev*, vol. 106, no. 9, pp. 4044–4098, Sep. 2006, doi: 10.1021/cr068360d.

[4] J. Rass-Hansen, H. Falsig, B. Jørgensen, and C. H. Christensen, “Bioethanol: fuel or feedstock?,” *Journal of Chemical Technology & Biotechnology*, vol. 82, no. 4, pp. 329–333, Apr. 2007, doi: 10.1002/jctb.1665.

[5] E. Furimsky, “Catalytic hydrodeoxygenation,” *Appl Catal A Gen*, vol. 199, no. 2, pp. 147–190, Jun. 2000, doi: 10.1016/S0926-860X(99)00555-4.

[6] C. H. Christensen, J. Rass-Hansen, C. C. Marsden, E. Taarning, and K. Egeblad, “The Renewable Chemicals Industry,” *ChemSusChem*, vol. 1, no. 4, pp. 283–289, Apr. 2008, doi: 10.1002/cssc.200700168.

[7] S. Kandasamy, S. P. Samudrala, and S. Bhattacharya, “The route towards sustainable production of ethylene glycol from a renewable resource, biodiesel waste: a review,” *Catal Sci Technol*, vol. 9, no. 3, pp. 567–577, 2019, doi: 10.1039/C8CY02035C.

[8] M.-Y. Zheng, A.-Q. Wang, N. Ji, J.-F. Pang, X.-D. Wang, and T. Zhang, “Transition Metal-Tungsten Bimetallic Catalysts for the Conversion of Cellulose into Ethylene Glycol,” *ChemSusChem*, vol. 3, no. 1, pp. 63–66, Jan. 2010, doi: 10.1002/cssc.200900197.

[9] Y. Zhang, A. Wang, and T. Zhang, “A new 3D mesoporous carbon replicated from commercial silica as a catalyst support for direct conversion of cellulose into ethylene glycol,” *Chem. Commun.*, vol. 46, no. 6, pp. 862–864, 2010, doi: 10.1039/B919182H.

[10] J. Pang, J. Sun, M. Zheng, H. Li, Y. Wang, and T. Zhang, “Transition metal carbide catalysts for biomass conversion: A review,” *Appl Catal B*, vol. 254, pp. 510–522, Oct. 2019, doi: 10.1016/j.apcatb.2019.05.034.

[11] G. Xu, A. Wang, J. Pang, M. Zheng, J. Yin, and T. Zhang, “Remarkable effect of extremely dilute H2SO4 on the cellulose conversion to ethylene glycol,” *Appl Catal A Gen*, vol. 502, pp. 65–70, Aug. 2015, doi: 10.1016/j.apcata.2015.05.038.

[12] H. Yue, Y. Zhao, X. Ma, and J. Gong, “Ethylene glycol: properties, synthesis, and applications,” *Chem Soc Rev*, vol. 41, no. 11, p. 4218, 2012, doi: 10.1039/c2cs15359a.

[13] M. Zheng, J. Pang, A. Wang, and T. Zhang, “One-pot catalytic conversion of cellulose to ethylene glycol and other chemicals: From fundamental discovery to potential commercialization,” *Chinese Journal of Catalysis*, vol. 35, no. 5, pp. 602–613, May 2014, doi: 10.1016/S1872-2067(14)60013-9.

[14] T.-L. Chen and D. R. Mullins, “Ethylene Glycol Adsorption and Reaction over CeO_X(111) Thin Films,” *The Journal of Physical Chemistry C*, vol. 115, no. 28, pp. 13725–13733, Jul. 2011, doi: 10.1021/jp201639n.

[15] C. A. Menning and J. G. Chen, “General trend for adsorbate-induced segregation of subsurface metal atoms in bimetallic surfaces,” *J Chem Phys*, vol. 130, no. 17, May 2009, doi: 10.1063/1.3125926.

[16] O. Skoplyak, M. A. Barteau, and J. G. Chen, “Reforming of Oxygenates for H_2 Production: Correlating Reactivity of Ethylene Glycol and Ethanol on Pt(111) and Ni/Pt(111) with Surface d-Band Center,” *J Phys Chem B*, vol. 110, no. 4, pp. 1686–1694, Feb. 2006, doi: 10.1021/jp0548927.

[17] JoséA. Rodriguez, “Physical and chemical properties of bimetallic surfaces,” *Surf Sci Rep*, vol. 24, no. 7–8, pp. 223–287, Jan. 1996, doi: 10.1016/0167-5729(96)00004-0.

[18] R. R. Davda, J. W. Shabaker, G. W. Huber, R. D. Cortright, and J. A. Dumesic, “Aqueous-phase reforming of ethylene glycol on silica-supported metal catalysts,” *Appl Catal B*, vol. 43, no. 1, pp. 13–26, Jun. 2003, doi: 10.1016/S0926-3373(02)00277-1.

[19] W. Yu, Z. J. Mellinger, M. A. Barteau, and J. G. Chen, “Comparison of Reaction Pathways of Ethylene Glycol, Acetaldehyde, and Acetic Acid on Tungsten Carbide and Ni-Modified Tungsten Carbide Surfaces,” *The Journal of Physical Chemistry C*, vol. 116, no. 9, pp. 5720–5729, Mar. 2012, doi: 10.1021/jp210756f.

[20] X. Guo, A. Hoffman, and J. T. Yates, “Adsorption kinetics and isotopic equilibration of oxygen adsorbed on the Pd(111) surface,” *J Chem Phys*, vol. 90, no. 10, pp. 5787–5792, May 1989, doi: 10.1063/1.456386.

[21] P. A. Redhead, “Thermal desorption of gases,” *Vacuum*, vol. 12, no. 4, pp. 203–211, Jul. 1962, doi: 10.1016/0042-207X(62)90978-8.

[22] J. L. Davis and M. A. Barteau, “Decarbonylation and decomposition pathways of alcohol’s on Pd(111),” *Surf Sci*, vol. 187, no. 2–3, pp. 387–406, Sep. 1987, doi: 10.1016/S0039-6028(87)80064-X.

[23] J. L. Davis and M. A. Barteau, “Decarbonylation and decomposition pathways of alcohol’s on Pd(111),” *Surf Sci*, vol. 187, no. 2–3, pp. 387–406, Sep. 1987, doi: 10.1016/S0039-6028(87)80064-X.

[24] S. M. Gates, J. N. Russell, and J. T. Yates, “Observation of a deuterium kinetic isotope effect in the chemisorption and reaction of methanol on Ni(111),” *Surf Sci*, vol. 146, no. 1, pp. 199–210, Oct. 1984, doi: 10.1016/0039-6028(84)90237-1.

[25] J. L. Davis and M. A. Barteau, “The influence of oxygen on the selectivity of alcohol conversion on the Pd(111) surface,” *Surf Sci*, vol. 197, no. 1–2, pp. 123–152, 1988, doi: 10.1016/0039-6028(88)90577-8.

[26] J. L. Davis and M. A. Barteau, “Reactions of carboxylic acids on the Pd(111)-(2 × 2)O surface: multiple roles of surface oxygen atoms,” *Surf Sci*, vol. 256, no. 1–2, pp. 50–66, Oct. 1991, doi: 10.1016/0039-6028(91)91199-8.

[27] J. L. Davis and A. Barteau, “Hydrogen Bonding in Carboxylic Acid Adlayers on Pd(lll): Evidence for Catemer Formation1 The adsorption of acetic acid and propanoic acid was studied on the Pd(lll) surface in order to gain,” *Langmuir*, vol. 5, pp. 1299–1309, 1989, Accessed: Aug. 20, 2023. [Online]. Available: https://pubs.acs.org/sharingguidelines

[28] M. Karatok, M. G. Sensoy, E. I. Vovk, H. Ustunel, D. Toffoli, and E. Ozensoy, "Formaldehyde Selectivity in Methanol Partial Oxidation on Silver: Effect of Reactive Oxygen Species, Surface Reconstruction, and Stability of Intermediates," *ACS Catal*, vol. 11, no. 10, pp. 6200–6209, May 2021, doi: 10.1021/acscatal.1c00344.

[29] J. L. Davis and M. A. Barteau, "Spectroscopic identification of alkoxide, aldehyde, and acyl intermediates in alcohol decomposition on Pd(111)," *Surf Sci*, vol. 235, no. 2–3, pp. 235–248, Sep. 1990, doi: 10.1016/0039-6028(90)90799-E.

[30] R. M. Williams, S. H. Pang, and J. W. Medlin, "O H versus C H bond scission sequence in ethanol decomposition on Pd(111)," *Surf Sci*, vol. 619, pp. 114–118, Jan. 2014, doi: 10.1016/j.susc.2013.09.014.

[31] I. E. Wachs and R. J. Madix, "The oxidation of ethanol on Cu(110) and Ag(110) catalysts," *Applications of Surface Science*, vol. 1, no. 3, pp. 303–328, May 1978, doi: 10.1016/0378-5963(78)90034-X.

[32] S. M. Gates, J. N. Russell, and J. T. Yates, "Bond activation sequence observed in the chemisorption and surface reaction of ethanol on Ni(111)," *Surf Sci*, vol. 171, no. 1, pp. 111–134, May 1986, doi: 10.1016/0039-6028(86)90565-0.

[33] E. Vesselli, A. Baraldi, G. Comelli, S. Lizzit, and R. Rosei, "Ethanol Decomposition: C□C Cleavage Selectivity on Rh(111)," *ChemPhysChem*, vol. 5, no. 8, pp. 1133–1140, Aug. 2004, doi: 10.1002/cphc.200400043.

[34] M. Li *et al.*, "Density Functional Study of Ethanol Decomposition on Rh(111)," *The Journal of Physical Chemistry C*, vol. 114, no. 49, pp. 21493–21503, Dec. 2010, doi: 10.1021/jp106856n.

[35] M. A. Barteau, J. Q. Broughton, and D. Menzel, "Vibrational spectroscopy of hydrocarbon intermediates on Ru(001)," *Applications of Surface Science*, vol. 19, no. 1–4, pp. 92–115, Nov. 1984, doi: 10.1016/0378-5963(84)90055-2.

[36] H. Steininger, H. Ibach, and S. Lehwald, "Surface reactions of ethylene and oxygen on Pt(111)," *Surf Sci*, vol. 117, no. 1–3, pp. 685–698, May 1982, doi: 10.1016/0039-6028(82)90549-0.

[37] J. L. Davis and M. A. Barteau, “Polymerization and decarbonylation reactions of aldehydes on the Pd(111) surface,” *J Am Chem Soc*, vol. 111, no. 5, pp. 1782–1792, Mar. 1989, doi: 10.1021/ja00187a035.

[38] C. Houtman and M. A. Barteau, “Reactions of formic acid and formaldehyde on Rh(111) and Rh(111)-(2 × 2)O surfaces,” *Surf Sci*, vol. 248, no. 1–2, pp. 57–76, May 1991, doi: 10.1016/0039-6028(91)90061-V.

[39] J. L. Davis and M. A. Barteau, “The interactions of oxygen with aldehydes on the Pd(111) surface,” *Surf Sci*, vol. 268, no. 1–3, pp. 11–24, Jan. 1992, doi: 10.1016/0039-6028(92)90946-4.

[40] M. A. Barteau, M. Bowker, and R. J. Madix, “Acid-base reactions on solid surfaces: The reactions of HCOOH, H2CO, and HCOOCH3 with oxygen on Ag(110),” *Surf Sci*, vol. 94, no. 2–3, pp. 303–322, Apr. 1980, doi: 10.1016/0039-6028(80)90009-6.

[41] E. M. Stuve, R. J. Madix, and B. A. Sexton, “An EELS study of the oxidation of H2CO on Ag(110),” *Surf Sci*, vol. 119, no. 2–3, pp. 279–290, Jul. 1982, doi: 10.1016/0039-6028(82)90297-7.

[42] M. Bowker and R. J. Madix, “XPS, UPS and thermal desorption studies of the reactions of formaldehyde and formic acid with the Cu(110) surface,” *Surf Sci*, vol. 102, no. 2–3, pp. 542–565, Jan. 1981, doi: 10.1016/0039-6028(81)90045-5.

[43] M. Salciccioli, W. Yu, M. A. Barteau, J. G. Chen, and D. G. Vlachos, “Differentiation of O–H and C–H Bond Scission Mechanisms of Ethylene Glycol on Pt and Ni/Pt Using Theory and Isotopic Labeling Experiments,” *J Am Chem Soc*, vol. 133, no. 20, pp. 7996–8004, May 2011, doi: 10.1021/ja201801t.

[44] R. J. Madix, T. Yamada, and S. W. Johnson, “The modification of surface reactivity by sulfur; Effects on dehydrogenation of ethanolamine, ethylene glycol, and acetaldehyde on Ni(100),” *Applications of Surface Science*, vol. 19, no. 1–4, pp. 43–58, Nov. 1984, doi: 10.1016/0378-5963(84)90052-7.

[45] M. M. M. Jansen, B. E. Nieuwenhuys, and H. Niemantsverdriet, “Chemistry of Ethylene Glycol on a Rh(100) Single-Crystal Surface,” *ChemSusChem*, vol. 2, no. 9, pp. 883–886, Sep. 2009, doi: 10.1002/cssc.200900153.

[46] N. F. Brown and M. A. Barteau, “Carbon-Halogen Bond Scission and Rearrangement of .beta.-Halohydrins on the Rh(111) Surface,” *J Phys Chem*, vol. 98, no. 48, pp. 12737–12745, 1994, doi: 10.1021/J100099A043.

[47] M. Bowker and R. J. Madix, “XPS, UPS and thermal desorption studies of alcohol adsorption on Cu(110): II. Higher alcohols,” *Surf Sci*, vol. 116, no. 3, pp. 549–572, May 1982, doi: 10.1016/0039-6028(82)90364-8.

[48] K. T. Queeney, C. R. Arumainayagam, M. K. Weldon, C. M. Friend, and M. Q. Blumberg, “Differential Reactivity and Structure of Mono-and Dialkoxides: The Reactions of Ethylene Glycol on Mo(110),” 1996, doi: https://doi.org/10.1021/ja953987r.

[49] M. B. Griffin, E. L. Jorgensen, and J. W. Medlin, “The adsorption and reaction of ethylene glycol and 1,2-propanediol on Pd(111): A TPD and HREELS study,” *Surf Sci*, vol. 604, no. 19–20, pp. 1558–1564, Sep. 2010, doi: 10.1016/j.susc.2010.05.025.

[50] K. T. Queeney, C. R. Arumainayagam, M. K. Weldon, C. M. Friend, and M. Q. Blumberg, “Differential Reactivity and Structure of Mono- and Dialkoxides: The Reactions of Ethylene Glycol on Mo(110),” *J Am Chem Soc*, vol. 118, no. 16, pp. 3896–3904, Apr. 1996, doi: 10.1021/ja953987r.

[51] A. J. Capote and R. J. Madix, “Carbon-carbon bond activation in the 1,2-ethanedioxy heterometallacycle by atomic oxygen on Ag(110),” *Surf Sci*, vol. 214, no. 1–2, pp. 276–288, Apr. 1989, doi: 10.1016/0039-6028(89)90423-8.

[52] X.-K. Gu, B. Liu, and J. Greeley, “First-Principles Study of Structure Sensitivity of Ethylene Glycol Conversion on Platinum,” *ACS Catal*, vol. 5, no. 4, pp. 2623–2631, Apr. 2015, doi: 10.1021/cs5019088.

[53] E. D. Wang, J. B. Xu, and T. S. Zhao, “Density Functional Theory Studies of the Structure Sensitivity of Ethanol Oxidation on Palladium Surfaces,” *The Journal of Physical Chemistry C*, vol. 114, no. 23, pp. 10489–10497, Jun. 2010, doi: 10.1021/jp101244t.

[54] A. J. Capote and R. J. Madix, “Oxygen-hydrogen and carbon-hydrogen bond activation in ethylene glycol by atomic oxygen on silver(110): heterometallacycle

formation and selective dehydrogenation to glyoxal," *J Am Chem Soc*, vol. 111, no. 10, pp. 3570–3577, May 1989, doi: 10.1021/ja00192a013.

[55] "Methanol Facts," Aug. 27, 2023. https://www.methanol.org/wp-content/uploads/2017/04/Formaldehyde-FS-Copy.pdf (accessed Aug. 27, 2023).

[56] J. W. Niemantsverdriet, *Spectroscopy in Catalysis*. Wiley, 2007. doi: 10.1002/9783527611348.

[57] M. K. Weldon and C. M. Friend, "Probing Surface Reaction Mechanisms Using Chemical and Vibrational Methods: Alkyl Oxidation and Reactivity of Alcohols on Transitions Metal Surfaces," *Chem Rev*, vol. 96, no. 4, pp. 1391–1412, Jan. 1996, doi: 10.1021/cr950224d.

[58] C. G. Freyschlag and R. J. Madix, "Precious metal magic: catalytic wizardry," *Materials Today*, vol. 14, no. 4, pp. 134–142, Apr. 2011, doi: 10.1016/S1369-7021(11)70085-2.

[59] "Dycor Dymaxion mass spectrometer - ametekpi.com," Aug. 20, 2023.

[60] A. Anil, O. F. Sadak, B. Karakurt, Y. Kocak, I. Lyubinetsky, and E. Ozensoy, "Interaction of CO_2 with MnO_x /Pd(111) Reverse Model Catalytic Interfaces," *ChemPhysChem*, vol. 24, no. 13, Jul. 2023, doi: 10.1002/cphc.202200787.

[61] A. Tamtögl, M. Kratzer, J. Killman, and A. Winkler, "Adsorption/desorption of H2 and CO on Zn-modified Pd(111)," *J Chem Phys*, vol. 129, no. 22, Dec. 2008, doi: 10.1063/1.3034126.

[62] S. J. Garrett, *"CHEM924 lecture notes, special topics in analytical chemistry-introduction to surface analysis*. 2001.

[63] X. Guo and J. T. Yates, "Dependence of effective desorption kinetic parameters on surface coverage and adsorption temperature: CO on Pd(111)," *J Chem Phys*, vol. 90, no. 11, pp. 6761–6766, Jun. 1989, doi: 10.1063/1.456294.

[64] "RBD Instruments Inc., United States of America, Oregon, Bend: Physics Today Buyer's Guide," Aug. 20, 2023.

[65] E. W. Wallace, "Mass Spectra," in *NIST Chemistry WebBook, NIST Standard Reference Database Number 69*, 2023.

[66] G. H. Gilmer and M. H. Grabow, “Models of Thin Film Growth Modes,” *JOM*, vol. 39, no. 6, pp. 19–23, Jun. 1987, doi: 10.1007/BF03258055.

[67] E. Vesselli, G. Comelli, R. Rosei, S. Freni, F. Frusteri, and S. Cavallaro, “Ethanol auto-thermal reforming on rhodium catalysts and initial steps simulation on single crystals under UHV conditions,” *Appl Catal A Gen*, vol. 281, no. 1–2, pp. 139–147, Mar. 2005, doi: 10.1016/j.apcata.2004.11.020.

[68] J. L. Davis and M. A. Barteau, “Hydrogen bonding in carboxylic acid adlayers on Pd(111): evidence for catemer formation,” *Langmuir*, vol. 5, no. 6, pp. 1299–1309, Nov. 1989, doi: 10.1021/la00090a004.

[69] J. L. Davis and M. A. Barteau, “The influence of oxygen on the selectivity of alcohol conversion on the Pd(111) surface,” *Surf Sci*, vol. 197, no. 1–2, pp. 123–152, 1988, doi: 10.1016/0039-6028(88)90577-8.

[70] F. Solymosi, A. Berkó, and T. I. Tarnóczi, “Adsorption and decomposition of methanol on Rh(111) studied by electron energy loss and thermal desorption spectroscopy,” *Surf Sci*, vol. 141, no. 2–3, pp. 533–548, Jun. 1984, doi: 10.1016/0039-6028(84)90147-X.